

# RSC Advances



This is an *Accepted Manuscript*, which has been through the Royal Society of Chemistry peer review process and has been accepted for publication.

*Accepted Manuscripts* are published online shortly after acceptance, before technical editing, formatting and proof reading. Using this free service, authors can make their results available to the community, in citable form, before we publish the edited article. This *Accepted Manuscript* will be replaced by the edited, formatted and paginated article as soon as this is available.

You can find more information about *Accepted Manuscripts* in the [Information for Authors](#).

Please note that technical editing may introduce minor changes to the text and/or graphics, which may alter content. The journal's standard [Terms & Conditions](#) and the [Ethical guidelines](#) still apply. In no event shall the Royal Society of Chemistry be held responsible for any errors or omissions in this *Accepted Manuscript* or any consequences arising from the use of any information it contains.



## Design and Synthesis of VEGFR-2 Tyrosine Kinase Inhibitors as Potential Anticancer Agents by Virtual Based Screening

Received 00th January 20xx,  
Accepted 00th January 20xx

DOI: 10.1039/x0xx00000x

[www.rsc.org/advances](http://www.rsc.org/advances)

Harun M. Patel <sup>†</sup>, Pankaj Bari <sup>‡</sup>, Rajshekhar Karpoormath <sup>†</sup>, Malleshappa Noolvi <sup>§</sup>, Neeta Thapliyal <sup>†</sup>, Sanjay Surana <sup>‡</sup>, Pritam Jain <sup>‡,\*</sup>

### Abstract

Vascular endothelial growth factor receptor-2 (VEGFR-2) plays a crucial role in cancer angiogenesis. A library of 6,7-dimethoxy quinazoline was prepared using ligand based drug design approach and passed through different filters of virtual screening such as docking study and Lipinski's rule. Twenty virtually screened compounds were synthesized and investigated against VEGFR-2 kinase and human umbilical vein endothelial cells (HUVEC) *in vitro*. Virtually screened compound **47** having 4-chlorophenyl-1,3,4-thiadiazole substitution at 3<sup>rd</sup> position of 6,7-dimethoxy-2-phenylquinazolin-4(3*H*)-one exhibited the most promising activity, with IC<sub>50</sub> value of 3.8 nm and 5.5 nm against VEGFR-2 tyrosine kinase and HUVEC cell line. Docking simulation supported the initial pharmacophoric hypothesis and suggested a common mode of interaction at the ATP-binding site of VEGFR-2 demonstrating that compound **47** was a potential agent for cancer therapy that deserves further research.

**Keywords:** 6,7-dimethoxy quinazoline, virtual screening, pharmacophore mapping, docking simulation, VEGFR-2.

Corresponding Author: P. S. Jain, E-mail: [pritash79@yahoo.com](mailto:pritash79@yahoo.com), Tel. No. : +91-2563-255189, Fax No.: +91-2563-251808

<sup>†</sup> Dept. of Pharmaceutical Chemistry, University of KwaZulu-Natal (Westville Campus), Private Bag X54001, Durban- 4000, South Africa.

<sup>‡</sup> Department of Pharmaceutical Chemistry, R.C. Patel College of Pharmacy, Shirpur, Dhule 425405, Maharashtra, India

<sup>§</sup> Department of Pharmaceutical Chemistry, Shree Dhanvantary Pharmacy College, Kim (Surat)-3941110, Gujrat, India

## 1. Introduction

Cancer management is an extremely challenging field for medicinal chemists to discover effective yet safer chemotherapeutic agents targeting various biochemical processes involved in progression of different kinds of cancers.<sup>1</sup> Among these targets, angiogenesis is one of the critical processes that affect growth and development of cancerous cells. Angiogenesis refers to generation of new blood vessels from the existing vasculature. It is the key factor in advancement of various human diseases, including cancer, where it is essential for the growth, spread and survival of tumors.<sup>2</sup> Angiogenesis is a complex process regulated by multiple growth factors and cytokines. Among these factors, vascular endothelial growth factor (VEGF) is one of the most potent angiogenic factors involved in tumor growth. It stimulates endothelial cell proliferation, migration and tube formation by binding to its two main receptor tyrosine kinases (RTKs) expressed on endothelial cells, VEGF receptor 1 (VEGFR-1) and VEGF receptor 2 (VEGFR-2).<sup>3</sup> Current evidence suggests that the interaction between VEGF and VEGFR-1 plays a minor role in angiogenesis, while VEGFR-2 mediates the major angiogenic function of VEGF.<sup>4</sup> Therefore, VEGF and VEGFR-2 have become therapeutic targets for the development of anticancer agents. Inhibition of the VEGFR-2 signalling pathway has an important anti-angiogenic effect on human cancer, which is evident from the approval of the small-molecule VEGFR-2 kinase inhibitors sorafenib (Bay 43-9006) [112],<sup>4</sup> sunitinib (SU-11248),<sup>5</sup> and pazopanib (GW786034)<sup>6</sup> by the Food and Drug Administration (FDA) for the treatment of advanced renal cell carcinoma.<sup>7</sup> Presently, many anti-angiogenic and multikinase agents are undergoing phase III clinical studies, including cediranib (AZD-2171) [16],<sup>8</sup> brivanib (BMS-582664),<sup>9</sup> axitinib (AG013736) [18]<sup>10</sup>, tivozanib (KRN-951) [19]<sup>11</sup>, and vandetanib (ZD-6474) [20].<sup>12</sup>

During the course of pharmaceutical development of novel VEGFR2 inhibitors, pharmacophore and docking based in silico studies are efficiently used to improve the discovery of lead identification and optimization, which is followed by the synthesis of lead compound derivatives and their biological evaluation. The discovery of pazopanib is an example of virtual screening using homology models and pharmacophore modeling.<sup>13</sup>

Inspired by this, in the current study, a library of quinazoline analogues was prepared using ligand based approach and passed through the different filters of virtual screening. Virtually screened hits were then synthesized and evaluated for their inhibitory activities against VEGFR-2 tyrosine kinase and VEGF-stimulated proliferation of HUVEC.

## 2. Virtual Screening Protocol

The virtual screening protocol used in this study is based on the application of sequential filters in order to select a restricted number of compounds to be submitted for biological evaluation. In the present study, both ligand based and structure based virtual screening approaches have been used. The workflow of the virtual screening campaign is outlined in **Fig. 1**. In detail, (i) a structure-based 3D pharmacophore model was optimized; (ii) a library of quinazoline analogs was made based upon the optimized pharmacophore; (iii) a structure-based 3D pharmacophore model was used as a search query on the quinazoline analogs (library), retaining the molecules that adhered to all the features of the model; (iii) the binding mode of all retrieved compounds was evaluated by molecular docking, using the 3D structure of VEGFR-2 tyrosine kinase; (iv) The next filter was Lipinski's rule of five to evaluate drug likeness, which becomes an essential tool to facilitate drug discovery. Finally, the virtually screened hits were synthesized and evaluated for their inhibitory activities against VEGFR-2 kinase and VEGF-stimulated proliferation of HUVEC.

## 2.1 Software and Hardware

Ligand based approach was carried out by the pharmacophore 3D-QSAR study using PHASE, version 3.0, Schrodinger, LLC, New York, USA, 2008.<sup>14</sup> PHASE supports various ligand-based drug design approaches like pharmacophore perception, structure alignment, 3D-QSAR and database searching.<sup>15</sup> Energy minimization of the dataset structures was accomplished using Macromodel with OPLS 2005 force field.<sup>16</sup> The minimized structures were imported in PHASE and appropriate protonation states were assigned to them at physiological pH  $7.2 \pm 2.0$  by Ligprep.<sup>17</sup> Different conformations were then generated using Confgen with OPLS 2001 force field using distance dependent dielectric solvation treatment.<sup>18</sup> Default pharmacophore features in PHASE include hydrogen bond acceptor (A), hydrogen bond donor (D), hydrophobic (H), negative (N), positive (P) and aromatic ring (R). It determines how molecular structure affects drug activity by dividing space into a fine cubic grid, encoding atom type occupation as numerical information, and performing a partial least-squares (PLS) regression, resulting in prediction of a significant model.<sup>15</sup> Structure based virtual screening was conducted using a graphical user interface XP-docking mode of program Maestro 8.<sup>19</sup> The protein structure of a complex VEGFR-2 was obtained from the RCSB Protein Data Bank (PDB) as entry 3B8Q (<http://www.rcsb.org/pdb/explore/explore.3B8Q>).<sup>20</sup> The protein was optimized for docking from its raw state employing protein preparation wizard with OPLS 2005 force field for minimization.<sup>21</sup> Receptor grid generation was accomplished using Glide. Further, we analyzed the compounds for Lipinski's rule of five to evaluate drug likeness using QikProp.

## 2.2 Ligand Based Drug Design

The novel 50 quinazoline derivatives were taken from literature<sup>22</sup> to derive pharmacophore based 3D QSAR model.<sup>22</sup> The  $IC_{50}$  values were converted to  $pIC_{50}$  using the formula ( $pIC_{50} = -\log IC_{50}$ ). Compounds that displayed insignificant or no inhibitions were excluded from the present study. The structures of all the compounds along with their actual and predicted biological activities are presented in **Table 1**. Three-dimensional (3D) conversion and minimization of 50 quinazoline ligands were performed using LigPrep (MMFFs force field) incorporated in PHASE. Conformers were generated using a rapid torsion angle search approach followed by minimization of each generated structure using the MMFFs force field, with an implicit GB/SA solvent model. A maximum of 1,000 conformers were generated per structure using a pre-process minimization of 1,000 steps and post process minimization of 500 steps. Each minimized conformer was filtered through the relative energy window of  $50 \text{ kJ mol}^{-1}$  and the minimum atom deviation of  $1.00 \text{ \AA}$ .<sup>23</sup> This value ( $50 \text{ kJ mol}^{-1}$ ) sets an energy threshold with respect to the lowest-energy conformer. Conformers having energy higher than the threshold are discarded. In order for two conformers to be considered identical, the distance between pairs of corresponding heavy atoms must be below  $1.00 \text{ \AA}$ . This rule is applied after the energy difference threshold, and only if the two conformers are within  $1 \text{ kcal mol}^{-1}$  of each other. The total set of inhibitors was divided randomly into a training set of 35 compounds for generation of 3D-QSAR models, and a test set of 15 compounds for validation of the developed model. The training set molecules were selected in such a way that they contained information in terms of both their structural features and biological activity range. The most active, moderately active and less active molecules were included, to spread out the range of activities.<sup>24</sup> Partial least-squares (PLS) regression analysis was applied to obtain the QSAR model. The maximum number of PLS factors were 5. PHASE QSAR models do not use internal cross-validation techniques, but rather use distinct training and test sets. PHASE supports only external validation, using an actual test set whose structures and activities are not considered when QSAR models are developed. Each of the developed 3D-QSAR models was validated by predicting activities of 15 test set molecules ( $q^2$ ). The predictive ability of the models was

measured by Pearson-R value. To overcome the over-fitting problem, the run was performed using 1-5 PLS factors, in which the standard deviation of regression was approximately equal to the experimental error. The stability value was used to check the strength of the resulting 3D QSAR model and compare models from the different hypotheses. The training set was used to identify the common pharmacophore hypothesis (CPH) by following tree-based partition algorithms. For finding the CPH, the dataset was divided into active and inactive sets depending upon the observed activity; active ligands are those with  $IC_{50}$  below 1.7 nm and inactive above 1.7 nm. Based on sites, maximum five features were allowed to develop hypotheses and a number of CPHs were reported that were common in all 50 molecules. Among the 147 hypotheses developed, five of them were selected for molecular alignment based upon the survival score. PLS analysis was conducted using five factors with a grid spacing of 1 Å and five regression models were derived. The pharmacophore hypothesis labelled as Models 1-5, together with their statistical scores, is listed in **Table 2**. Based on  $r^2$ ,  $q^2$ , SD and RMSE, as well as on the highest value on the Pearson-R, Model-I was found to be the best model ( $r^2 = 0.9687$ ,  $q^2 = 0.7106$ ,  $F = 148.6$ ). The graph of observed versus predicted biological activity of training and test sets are shown in **Fig. 2**. The pharmacophore model hypothesis distances and angles are depicted in **Fig. 3** and respectively. **Table 3** displayed the alignment of active compounds in accordance with the hypothesis. For Model-I, the training set correlation is characterized by PLS factors ( $r^2 = 0.9687$ ,  $SD = 0.1969$ ,  $F = 148.6$ ,  $P = 0.8709$ ). The test set correlation is characterized by PLS factors ( $q^2 = 0.7106$ ,  $RMSE = 0.4487$ ,  $Pearson-R = 0.8709$ ). The contribution maps obtained from Model-I AAARR.8 show how 3D-QSAR methods can identify features important for the interaction between ligands and their target protein.

### 2.3 Designing of the Library based upon Ligand based Strategy

The library was designed based on the developed 3D-QSAR models and earlier reported work on quinazoline based inhibitors of VEGFR-2. Among them, Model-I was found to be significantly more accurate, characterized by PLS factors ( $r^2 = 0.9687$ ,  $SD = 0.1969$ ,  $F = 148.6$ ,  $P = 0.8709$ ) and the test set correlation is characterized by PLS factors ( $q^2 = 0.7106$ ,  $RMSE = 0.4487$ ,  $Pearson-R = 0.8709$ ). The resulting 3D-QSAR contour maps provide useful insights in active-structure relationship, allowing a discussion in terms of drug design. N-1, 6 and 7 alkoxy oxygen of quinazoline ring served as hydrogen bond acceptor (**A1**, **A3** and **A4 respectively**) in drug receptor interaction. Ring residue, **R13**, in this model occupies much of the favourable blue cubes due to the presence of hydrophobic quinazoline ring. Similarly, ring residues, **R15**, suggest that bulky substituent is essential for producing VEGFR-2 kinase inhibition as shown in **Fig. 3** and **4**.

Our strategy is directed towards designing a variety of ligands with diverse chemical properties as per the developed 3D QSAR pharmacophore model hypothesizing that the potency of these molecules might be enhanced by adding an alternative binding group such as phenyl at 2<sup>nd</sup> position, and substituted thiadiazoles, oxadiazoles, different amines and substituted hydrazides at 3<sup>rd</sup> position of the 6,7-dimethoxy quinazoline ring. In this way, such a substitution pattern could target various regions of the ATP-binding site of the protein kinase domain to create differentially selective molecules. Based upon pharmacophore based 3D-QSAR and literature survey of VEGFR-2 inhibitors, we designed the library of 75 compounds as shown in **Fig. 5**, **6(A)**, **6(B)** and **6(C)**.

### 2.4 Structure Based Drug Design

The molecular docking tool, GLIDE<sup>25</sup> was used for ligand docking studies into the VEGFR-2 tyrosine kinase receptor binding pocket. The crystal structure of VEGFR-2 tyrosine kinase was obtained from the protein data bank, PDB ID: 3B8Q. The protein preparation was carried out using 'protein preparation wizard' in Maestro 8.0 in two steps, preparation and refinement. After ensuring chemical correctness, water

molecules in the crystal structures were deleted, and hydrogens were added, wherever they were missing. The energy of crystal structure was minimized.<sup>26</sup> Grids were defined centering them on the ligand in the crystal structure using the default box size. The ligands were developed using maestro build panel and prepared by Ligprep 2.2 module that produces the low energy conformer of ligands using OPLS 2005 force field.<sup>27</sup> The low energy conformation of the ligands was selected and docked into the grid generated from protein structures using standard precision (SP) docking mode. The final evaluation was done with glide score (docking score), and a single best pose is generated as the output for a particular ligand. 6,7-dimethoxy quinazoline analogues were modeled by positioning them in the co-crystallized ligand's binding site. The entire complex was subjected to alternate cycles of minimization and dynamics. The co-crystallized ligand was re-docked into the active site of the enzyme and then replaced with 6,7-dimethoxy quinazoline derivatives in order to compare the binding mode of both co-crystallized ligand and the compounds under investigation.

### 2.5 Lipinski's Rule for Drug Likelihood

Pharmacokinetic property optimization is a rather complex undertaking that is likely to require changes in those molecular determinants that are responsible for binding affinity and specificity like hydrogen bonds. It is well known that numerous drug candidates have failed during clinical tests because of problems related to ADME (absorption, distribution, metabolism and excretion) properties. We analyzed physically significant descriptors and pharmaceutically relevant properties such as molecular weight, log p, H-bond donors and H-bond acceptors of all the synthesized compounds, according to Lipinski's rule of five. Hydrogen bond acceptor (HBA) and hydrogen bond donor (HBD) groups in the compound optimize the drug receptor interaction. Lipinski's rule of five is a rule of thumb to evaluate drug likeness, or determine if a chemical compound with a certain pharmacological or biological activity has properties that would most likely make it an orally active drug in humans. The rule describes delicate balance between the molecular properties of a compound, which directly influence its pharmacodynamics and pharmacokinetics, and ultimately affect their ADME in the human body like a drug. In general, these parameters allow to ascertain poor oral absorption or membrane permeability that occurs when the evaluated molecules present values higher than five H-bond donors (HBD), 10 H-bond acceptors (HBA), molecular weight (MW) > 500 Da and LogP (cLogP) > 5 (Lipinski's 'rule-of-five').<sup>28</sup> We also evaluated the number of violations of Lipinski's rule of five. Compounds that satisfy these rules are considered as drug like. Compounds with fewer (and preferably no) violations of these rules are more likely to be orally available.

### 3. Chemistry

The synthesis of virtually screened 6,7-dimethoxy quinazoline analogues was achieved through an efficient and versatile synthetic route, as illustrated in **Scheme 1** and **2**. It is quite clear that unique final steps were involved in the synthesis of target compounds, having structural variations at the 3<sup>rd</sup> position of 6,7-dimethoxy quinazoline ring. Reaction of equimolar quantity of 4,5-dimethoxy anthranilic acid (**A**) with benzoyl chloride (**B**) in dry pyridine yielded 6,7-dimethoxy-2-phenyl-4H-benzo[d][1,3]oxazin-4-one(**C**) by *N*-benzoylation via dehydrative cyclization mechanism. Subsequently, 6,7-dimethoxy-2-phenyl-4H-benzo[d][1,3]oxazin-4-one(**C**) reacted with different substituted primary amines containing oxadiazole/ thiazadiazoles/ anilines in dry pyridine to obtain the virtually screened compounds as shown in **Scheme 1** and **2**. Benzoxazinones undergo ring opening with different nucleophiles, allowing incorporation of substitution at the 3<sup>rd</sup> position. Hence, the use of dry pyridine and maintenance of anhydrous condition is mandatory, while synthesizing the above-mentioned analogues. It is also reported that the benzoxazinones are liable to hydrolysis by water.<sup>29</sup> The actual extent to which this hydrolysis occurs varies greatly across a range of



molecules. A molecule of water opens the benzoxazinone ring by attacking the intracyclic carbonyl and effectively hydrolyzing the cyclic ester (**Fig. 7**). Hence, the pyridine should be completely dry.<sup>29</sup>

It is also suggested that the nature of the substitution on the benzoxazinone can modulate the reactivity of the carbonyl, such as the electron donating groups cause the carbonyl to be less electrophilic and reduce the reactivity of the benzoxazinone carbonyl to nucleophilic attack.<sup>30</sup>

This is desirable in terms of stability on storage, or if they are to be the final molecules themselves, it also being a factor when these molecules are altered for further analogue production.

An alkyl chain act as an electron donor (+I effect), suggesting that the longer the chain gets, the reaction and insertion of the group that constitute the substitution at the 3<sup>rd</sup> position of the corresponding 6,7-dimethoxy quinazoline becomes more difficult (**Fig. 8**).

All the newly synthesized compounds exhibited acceptable analysis of their anticipated structures, which have been summarized in experimental section. In general, the IR spectrum of all virtually screened compounds revealed typical absorption bands around 1640-1695 cm<sup>-1</sup> for C=O (of 6,7-dimethoxy quinazoline at 4<sup>th</sup> position) and 1531-1563 cm<sup>-1</sup> for C=N, which confirms the formation of 6,7-dimethoxy quinazoline ring. <sup>1</sup>H NMR spectrum of virtually screened compounds exposed the characteristic two methoxy peak at 3.91-3.92 δ ppm and 3.93-3.98 δ ppm, which is magnetically different. This was further confirmed from <sup>13</sup>C NMR spectrum that exhibited two methoxy peaks at 56.12δ ppm and 56.41δ ppm. The mass spectra of these compounds additionally confirmed the assigned structures.

#### 4. Results and Discussion

In the beginning, a reported series of 6,7-dimethoxy quinazoline derivatives with VEGFR-2 tyrosine kinase inhibitory activity was subjected to a 3D-QSAR study. All the developed 3D-QSAR models showed good predictabilities and statistical validation. Model-I was significantly more accurate than other models and was characterized by PLS factors ( $r^2 = 0.9687$ ,  $SD = 0.1969$ ,  $F = 148.6$ ,  $P = 0.8709$ ). The test set correlation was characterized by the PLS factors ( $q^2 = 0.7106$ ,  $RMSE = 0.4487$ ,  $Pearson-R = 0.8709$ ). The resulting 3D-QSAR contour maps provide useful insights in active-structure relationship, allowing a discussion in terms of drug design. Nitrogen atom of 6,7-dimethoxy quinazoline ring served as hydrogen bond acceptor (A1) in drug receptor interaction. Ring residue (R13) in this model occupies much of the favourable blue cubes due to the presence of hydrophobic 6,7-dimethoxy quinazoline ring. Similarly ring residue (R15) suggests that bulky substituent is essential for producing VEGFR-2 kinase inhibition. It is also inferred from the docking results that the bulky moiety is located in a deep hydrophobic pocket. Hydrogen bond acceptor (A3 and A4) at 6<sup>th</sup> and 7<sup>th</sup> position of quinazoline ring indicates that electron donating substituent methoxy is favourable for VEGFR-2 inhibition activity, as shown in **Fig. 3** and **4**.

As per the pharmacophore based 3D-QSAR and literature survey of VEGFR-2 inhibitors, we designed the library of 75 compounds. Designed library was passed through the developed 3D-QSAR model to validate the designing. Among the 75 compounds, 51 compounds showing significant predicted activity ( $IC_{50}$  below 5.17) were further selected for next filter of docking study, as shown in Table 4.

Docking studies revealed that the quinazoline ring binds to a narrow hydrophobic pocket in the N-terminal domain of VEGFR-2 tyrosine kinase where N-1 of the quinazoline ring interacts with H-atom of amino acid backbone of CYS-919 via a hydrogen bond. These interactions underscore the importance of both nitrogen atoms for binding and the subsequent inhibitory capacity. 6,7-dimethoxy quinazoline ring is surrounded by the hydrophobic residue such as Val848, Lys868, Thr916, indicating its role in hydrophobic interaction, with the ring residue (R13) in 3D QSAR model also suggesting the same. The thiadiazoles/ oxadiazole/ aniline moiety at C-3 position of 6,7-dimethoxy

quinazoline is observed to be inserted deeply in the cavity, interacting with Leu840, Ala866, Phe918 and Phe1047 through hydrophobic interaction, as shown in **Fig. 9, 10 and 11**. The ring residue (R15) also confirms the hydrophobic interaction of thiadiazoles/ oxadiazole/ aniline moiety in the 3D-QSAR study. This deep cavity is very well conserved in all tyrosine kinase iso forms and coincides with the ATP-binding site region. As a measure of docking reliability, the docking results are evaluated in terms of glide dock score values by comparison of the docked poses of the co-crystallized ligand. Compounds having docking score above -5.77 are allowed for the next filter of lipinski's rule. Out of 51 compounds, 27 compounds show good docking score and glide energy, as depicted in **Fig. 9, 10, 11 and Table 5**. We further analyzed virtually filtered 27 compounds for Lipinski's rule of five. The rule describes molecular properties important for a drug's pharmacokinetics in the human body, including its ADME. Although the cytotoxic effects of lead compounds are thought to be primarily due to their ability to modulate cell death, other factors such as solubility, stability and/ or efflux properties within the cell may also contribute. The QikProp 3.2 is used to analyze drug likeness (Lipinski's Rule of Five), and the results are given in Table 6. It was found that all the synthesized compounds comply with these rules, except for 28, 31, 32, 44, 61, 70 and 72, which did not comply for molecular weight and QPlogP O/W, showing violation of Lipinski's Rule of Five.

Finally, 20 virtually screened compounds are further synthesized, as shown in Scheme 1 and 2. The reaction of 4,5-dimethoxy anthranilic acid (**A**) and benzoyl chloride (**B**) in dry pyridine afforded 6,7-dimethoxy-2-phenyl-4H-benzo[d][1,3]oxazin-4-one (**C**) (**Scheme 1 and 2**). **C** was refluxed with different substituted thiadiazoles, oxadiazoles and anilines containing primary amine to obtain the desired compounds. While synthesizing virtually screened compounds, the quinazoline ring opened and two products, a 90% closed ring and a 10% open ring product, i.e. diamides, were obtained, as shown in **Scheme 3**.

Following are some of the predictions and the reasons that probably caused this opening and closing of the ring. The substituents have a dominant bearing on the reactivity of the benzoxazinone carbonyl and the electronic contribution, in particular, of the ring substituents seems to dominate. The order of reactivity was observed to follow the trend of the electronic contribution of the substituents through either induction, resonance or a combination of the two. Conversely, if there is an N-N type molecule acting as the nucleophile, the factor that determines which nitrogen attacks is most probably the steric effect, rather than nucleophilicity. The least hindered nitrogen, rather than the most nucleophiles, attacks the carbonyl. This information is valuable if a range of nitrogen nucleophiles are used in the formation of quinazolines and may explain differing yields of final product. Thus, the benzoxazinone molecule was useful as there was potential to introduce diversity into the system at specific points by simply changing the nature of the starting materials. It is shown that the molecule undergoes ring opening with different nucleophiles allowing incorporation of substitution at the 3rd position. This in turn generates a number of molecules for the SAR study. One of the main reasons that these molecules did not easily purify was due to their potential to degrade when exposed to water. It is known that the benzoxazinones are liable to hydrolysis by water and the increase in stability of 2-alkylbenzoxazinones is related to the length of the side chain. The actual extent to which this hydrolysis occurs varies greatly across a range of molecules. A molecule of water opens the benzoxazinone ring by attacking the intracyclic carbonyl and effectively hydrolyzes the cyclic ester as shown in **Fig. 7**.

All the virtually synthesized compounds were tested for VEGFR-2 kinase activity using homogeneous time resolved fluorescence (HTRF) method.<sup>31</sup> The catalytic activity of kinases was measured by phosphorylated biotin-peptide conjugate using streptavidin linked-APC and



europium-labelled anti-phosphotyrosine antibody. Subsequently, a cell proliferation assay was performed to find the potent VEGFR-2 kinase inhibitors among these compounds for their ability to inhibit VEGF-stimulated proliferation of HUVEC 39, with the results being shown in **Table 7**. Overall, considerable relationships between their structures and inhibitory activities were observed.

With respect to the VEGFR-2 inhibition assay, all compounds elicited moderate to significant kinase inhibition activity with  $IC_{50}$  values in the range of 3.8-124 nM. Regarding the SAR findings of 6,7-dimethoxy quinazoline analogues, it is observed that thiadiazole derivatives are more potent as compared to the oxadiazole and aniline at 3rd position of 6,7-dimethoxy-2-phenylquinazolin-4(3H)-one. Among the virtually screened compounds, compound 47 with 4-chlorophenyl-1,3,4-thiadiazole substitution at 3rd position of 6,7-dimethoxy-2-phenylquinazolin-4(3H)-one exhibited most promising activity, with  $IC_{50}$  value of 3.8 nM against VEGFR-2 tyrosine kinase and 5.5 nM against the HUVEC cell line. Less bulky hydrophobic substitution on 5th position of 1,3,4-thiadiazole and 1,3,4-oxadiazole decreases the activity (compound 21, 46), indicating that optimum hydrophobicity is required at 5th position to have VEGFR-2 inhibition activity.

Within set of 1,3,4-oxadiazole substituted quinazoline derivatives, it was found that presence of electron withdrawing group on phenyl ring at 5th position of 1,3,4-oxadiazole increases the activity and vice versa, which is obvious by observing the VEGFR-2 inhibition of compound 22 ( $IC_{50}$ =12 nM, 4-Cl substituted) and 26 ( $IC_{50}$ =107 nM, 3-methyl substituted). By comparing the VEGFR-2 inhibition of compound 23 ( $IC_{50}$ =15 nM) and 40 ( $IC_{50}$ =13.5 nM), it is concluded that para-methoxy is more active than ortho on phenyl ring at 5th position of 1,3,4-oxadiazole and same thing is also observed with aniline series, where para-methoxy aniline (compound 10,  $IC_{50}$ =13.5 nM) is more active than ortho-methoxy aniline (compound 2,  $IC_{50}$ =13.5 nM).

## 5. Conclusion

In conclusion, virtually screened twenty 6,7-dimethoxy quinazoline derivatives were synthesized by ligand based and structured based drug design approach. With respect to the VEGFR-2 inhibition assay, all compounds elicited moderate to significant kinase inhibition activity with  $IC_{50}$  values in the range of 3.8-124 nM. Among the virtually screened compounds, compound 47 with 4-chlorophenyl-1,3,4-thiadiazole substitution at 3rd position of 6,7-dimethoxy-2-phenylquinazolin-4(3H)-one exhibited most promising activity with  $IC_{50}$  value of 3.8 nM against VEGFR-2 tyrosine kinase and 5.5 nM against the HUVEC cell line. Docking studies revealed that the quinazoline ring binds to a narrow hydrophobic pocket in the N-terminal domain of VEGFR-2 tyrosine kinase where N-1 of the quinazoline ring interacts with H-atom of amino acid backbone of CYS-919 via a hydrogen bond. These interactions underscore the importance of both nitrogen atoms for binding and the subsequent inhibitory capacity. Regarding the SAR findings of 6,7-dimethoxy quinazoline analogues, it is seen that thiadiazole derivatives are more potent as compared to the oxadiazole and aniline at 3rd position of 6,7-dimethoxy-2-phenylquinazolin-4(3H)-one. The overall outcome of this model revealed that optimum hydrophobicity is required at 5th position to have VEGFR-2 inhibitory activity. Within set of 1,3,4-oxadiazole substituted quinazoline derivatives, it was found that presence of electron withdrawing group on phenyl ring at 5th position of 1,3,4-oxadiazole increases the activity and vice versa. These encouraging results of biological screening of the tested compounds offer an excellent framework in this field that may lead to discovery of potent VEGFR-2 inhibitors. Finally, it is conceivable that further derivatization of such compounds will be of interest with the hope to get more selective and potent VEGFR-2 inhibitors.

## 6. Experimental

All the chemicals and solvents were supplied by Sigma-Aldrich and Spectrochem Pvt. Ltd. Solvents were distilled and dried before use as required. The reactions were monitored with the help of thin-layer chromatography using pre-coated aluminium sheets with GF254 silica gel, 0.2 mm layer thickness (Merck) by using solvent systems benzene : acetone (7:3 and 9:1) and toluene: ethyl acetate: formic acid (5:4:1). The spots were visualized under UV lamp. Melting points of the synthesized compounds were determined and are uncorrected using one end open capillary tubes on a scientific melting point apparatus, Analab Scientific Instruments. FTIR spectrum was recorded using KBr on FTIR-8400S Shimadzu spectrometer. <sup>1</sup>H NMR (DMSO) spectra of the synthesized compounds were performed with Bruker Avance-II 400 NMR spectrometer operating at 400 MHz in SAIF, Punjab University, Chandigarh. Chemical shifts were measured relative to internal standard TMS and are reported in  $\delta$  ppm. Mass spectra of the synthesized compounds were recorded at MAT 120 in SAIF, Punjab University.

### 6.1 Synthesis of 6,7-dimethoxy-2-phenyl-4H-benzo[d][1,3]oxazin-4-one (C)

An equimolar quantity of 4,5-dimethoxy anthranilic acid (A) and benzoyl chloride (B) was stirred in dry pyridine at 0-5°C for 1 hr, to get the solid product. Obtained solid was washed with dil. HCl to remove excess pyridine and with sodium bicarbonate solution to remove excess benzoyl chloride. It was further recrystallized from ethanol to get the pure compound C.<sup>32</sup>

### 6.2 General procedure for the synthesis of virtually screened compounds

Equimolar quantity of 6,7-dimethoxy-2-phenyl-4H-benzo[d][1,3]oxazin-4-one (C) and different substituted primary amines containing oxadiazole/ thiadiazoles/ anilines in dry pyridine was added slowly and reaction mixture was refluxed for 24 hrs. The mixture so obtained was added to crushed ice and the separated precipitate was filtered off and washed with dil. HCl. Recrystallization was carried out from ethanol. All the compounds were further purified by column chromatography using Benzene: Acetone (7:3) as eluant.

#### 6.2.1 6,7-dimethoxy-3-(2-methoxyphenyl)-2-phenylquinazolin-4(3H)-one (2)

This compound was prepared and purified as per the above mentioned procedure: yield 62 %; mp 288-291 °C. IR (KBr,  $\nu_{\max}$ ,  $\text{cm}^{-1}$ ): 2957.97 (CH), 1640.54 (C=O), 1545.12 (C=N); <sup>1</sup>H NMR (DMSO-d<sub>6</sub>)  $\delta$  ppm: 3.91-3.92 (s, magnetically different, 3H, OCH<sub>3</sub>), 3.93-3.98 (s, magnetically different 3H, OCH<sub>3</sub>), 3.83 (s, 3H, OCH<sub>3</sub>), 6.98-8.09 (m, 11H, Ar-H); <sup>13</sup>C NMR (DMSO-d<sub>6</sub>)  $\delta$  ppm: 55.21, 56.12, 56.41, 106.43, 108.48, 114.36, 115.37, 116.38, 118.38, 125.29, 126.23, 128.67, 128.87, 128.92, 132.47, 143.56, 155.57, 156.47, 154.38, 156.58, 163.77; HRMS (EI) m/z calcd for C<sub>23</sub>H<sub>20</sub>N<sub>2</sub>O<sub>4</sub>: 388.1423; found: 388.1428.

#### 6.2.2 3-(4-chlorophenyl)-6,7-dimethoxy-2-phenylquinazolin-4(3H)-one (3)

This compound was prepared and purified as per the above mentioned procedure: yield 62 %; mp 288-291 °C. IR (KBr,  $\nu_{\max}$ ,  $\text{cm}^{-1}$ ): 2924.18 (CH), 1673.30 (C=O), 1538.23 (C=N), 768.66 (C-Cl); <sup>1</sup>H NMR (DMSO-d<sub>6</sub>)  $\delta$  ppm: 3.91-3.92 (s, magnetically different, 3H, OCH<sub>3</sub>), 3.93-3.98 (s, magnetically different 3H, OCH<sub>3</sub>) 7.02-8.09 (m, 11H, Ar-H); <sup>13</sup>C NMR (DMSO-d<sub>6</sub>)  $\delta$  ppm: 56.12, 56.41, 108.73, 109.47, 116.47, 125.13, 128.53, 128.90, 129.45, 130.14, 130.03, 131.00, 133.56, 146.24, 152.17, 153.56, 158.58, 163.26; HRMS (EI) m/z calcd for C<sub>22</sub>H<sub>17</sub>ClN<sub>2</sub>O<sub>3</sub>: 392.0928; found: 392.0932

#### 6.2.3 6,7-dimethoxy-3-(4-methoxyphenyl)-2-phenylquinazolin-4(3H)-one (10)

This compound was prepared and purified as per the above mentioned procedure: yield 62 %; mp 288-291 °C. IR (KBr,  $\nu_{\max}$ ,  $\text{cm}^{-1}$ ): 2923.27 (CH), 1672.34 (C=O), 1531.34 (C=N); <sup>1</sup>H NMR (DMSO-d<sub>6</sub>)  $\delta$  ppm: 3.91-3.92 (s, magnetically different, 3H, OCH<sub>3</sub>), 3.93-3.98 (s,

magnetically different 3H, OCH<sub>3</sub>), 3.89 (s, 3H, OCH<sub>3</sub>), 6.70-7.88 (m, 11H, Ar-H); <sup>13</sup>C NMR (DMSO-d<sub>6</sub>) δ ppm: 55.81, 56.12, 56.41, 108.45, 109.57, 115.47, 116.12, 126.48, 127.24, 128.62, 128.82, 128.90, 132.37, 146.46, 154.16, 156.11, 157.47, 158.53, 163.91; HRMS (EI) m/z calcd for C<sub>23</sub>H<sub>20</sub>N<sub>2</sub>O<sub>4</sub>: 388.1423; found: 388.1419

#### 6.2.4 6,7-dimethoxy-2,3-diphenylquinazolin-4(3H)-one (14)

This compound was prepared and purified as per the above mentioned procedure: yield 62 %; mp 288-291 °C. IR (KBr, ν<sub>max</sub>, cm<sup>-1</sup>):2924.18 (CH), 1663.78 (C=O), 1552.12 (C=N); <sup>1</sup>H NMR (DMSO-d<sub>6</sub>) δ ppm: 3.91-3.92 (s, magnetically different, 3H, OCH<sub>3</sub>), 3.93-3.98 (s, magnetically different 3H, OCH<sub>3</sub>) 7.14-8.28 (m, 12H, Ar-H); <sup>13</sup>C NMR (DMSO-d<sub>6</sub>) δ ppm: 56.12, 56.41, 107.62 108.45, 116.47, 124.67, 125.35, 126.35, 127.16, 128.34, 128.48, 131.47, 132.46, 146.24, 154.08, 155.12, 156.46, 163.48; HRMS (EI) m/z calcd for C<sub>22</sub>H<sub>18</sub>N<sub>2</sub>O<sub>3</sub>: 358.1317; found: 358.1322.

#### 6.2.5 6,7-dimethoxy-3-(5-methyl-1,3,4-oxadiazol-2-yl)-2-phenylquinazolin-4(3H)-one (21)

This compound was prepared and purified as per the above mentioned procedure: yield 62 %; mp 288-291 °C. IR (KBr, ν<sub>max</sub>, cm<sup>-1</sup>):2978. (Aro-CH), 2924.18 (Alc-CH), 1685.69 (C=O), 1561.24 (C=N); <sup>1</sup>H NMR (DMSO-d<sub>6</sub>) δ ppm: 2.61 (s, 3H, CH<sub>3</sub>), 3.91-3.92 (s, magnetically different, 3H, OCH<sub>3</sub>), 3.93-3.98 (s, magnetically different 3H, OCH<sub>3</sub>) 7.12-8.24 (m, 11H, Ar-H); <sup>13</sup>C NMR (DMSO-d<sub>6</sub>) δ ppm: 20.23, 56.12, 56.41, 109.57, 110.58, 116.58, 128.21, 128.45, 128.72, 130.56, 146.45, 154.18, 155.42, 156.43, 163.56, 164.87, 170.64; HRMS (EI) m/z calcd for C<sub>19</sub>H<sub>16</sub>N<sub>4</sub>O<sub>4</sub>: 364.1172; found: 364.1176

#### 6.2.6 3-(5-(4-chlorophenyl)-1,3,4-oxadiazol-2-yl)-6,7-dimethoxy-2-phenylquinazolin-4(3H)-one (22)

This compound was prepared and purified as per the above mentioned procedure: yield 62 %; mp 288-291 °C. IR (KBr, ν<sub>max</sub>, cm<sup>-1</sup>): 2990.73 (CH), 1668.66 (C=O), 1541.78 (C=N), 762.12 (C-Cl); <sup>1</sup>H NMR (DMSO-d<sub>6</sub>) δ ppm: 3.91-3.92 (s, magnetically different, 3H, OCH<sub>3</sub>), 3.93-3.98 (s, magnetically different 3H, OCH<sub>3</sub>) 7.18-8.42 (m, 11H, Ar-H); <sup>13</sup>C NMR (DMSO-d<sub>6</sub>) δ ppm: 56.12, 56.41, 108.34, 110.56, 114.56, 125.78, 126.34, 127.12, 128.00, 128.31, 129.72, 130.46, 134.46, 146.46, 154.27, 155.13, 156.28, 163.72, 164.37, 170.18; HRMS (EI) m/z calcd for C<sub>24</sub>H<sub>17</sub>ClN<sub>4</sub>O<sub>4</sub>: 460.0938; found: 462.0933.

#### 6.2.7 6,7-dimethoxy-3-(5-(2-methoxyphenyl)-1,3,4-oxadiazol-2-yl)-2-phenylquinazolin-4(3H)-one (23)

This compound was prepared and purified as per the above mentioned procedure: yield 62 %; mp 288-291 °C. IR (KBr, ν<sub>max</sub>, cm<sup>-1</sup>):2989.76 (CH), 1679.81 (C=O), 1556.24 (C=N); <sup>1</sup>H NMR (DMSO-d<sub>6</sub>) δ ppm: 3.91-3.92 (s, magnetically different, 3H, OCH<sub>3</sub>), 3.93-3.98 (s, magnetically different 3H, OCH<sub>3</sub>), 3.89 (s, 3H, OCH<sub>3</sub>), 7.02-8.09 (m, 11H, Ar-H); <sup>13</sup>C NMR (DMSO-d<sub>6</sub>) δ ppm: 55.62, 56.12, 56.41, 108.37, 109.28, 112.38, 115.12, 118.13, 121.28, 124.12, 128.38, 128.67, 129.38, 131.28, 133.88, 144.37, 153.12, 154.45, 156.45, 157.23, 163.12, 164.47, 169.72; HRMS (EI) m/z calcd for C<sub>25</sub>H<sub>20</sub>N<sub>4</sub>O<sub>5</sub>: 456.1434; found: 456.1438.

#### 6.2.8 3-(5-cyclopropyl-1,3,4-oxadiazol-2-yl)-6,7-dimethoxy-2-phenylquinazolin-4(3H)-one (24)

This compound was prepared and purified as per the above mentioned procedure: yield 62 %; mp 288-291 °C. IR (KBr, ν<sub>max</sub>, cm<sup>-1</sup>): 2940.58 (CH), 1650.24 (C=O), 1538.24 (C=N). <sup>1</sup>H NMR (DMSO-d<sub>6</sub>) δ ppm: 1.14-2.50 (m, 5H, cyclopropyl), 3.91-3.92 (s, magnetically different, 3H, OCH<sub>3</sub>), 3.93-3.98 (s, magnetically different 3H, OCH<sub>3</sub>) 7.02-8.09 (m, 11H, Ar-H); <sup>13</sup>C NMR (DMSO-d<sub>6</sub>) δ ppm: 8.21, 9.25, 56.12, 56.41, 108.52, 109.87, 116.12, 128.17, 128.56, 128.74, 131.98, 145.45, 153.86, 154.45, 158.34, 163.87, 165.34, 170.87; HRMS (EI) m/z calcd for C<sub>21</sub>H<sub>18</sub>N<sub>4</sub>O<sub>4</sub>: 390.1328; found: 390.1333.

**6.2.9 6,7-dimethoxy-2-phenyl-3-(5-m-tolyl-1,3,4-oxadiazol-2-yl)quinazolin-4(3H)-one (26)**

This compound was prepared and purified as per the above mentioned procedure: yield 62 %; mp 288-291 °C. IR (KBr,  $\nu_{\text{max}}$ ,  $\text{cm}^{-1}$ ): 2924.18 (Ar-CH), 2901.45 (Ali-CH), 1662.34 (C=O), 1539.12 (C=N);  $^1\text{H}$  NMR (DMSO- $d_6$ )  $\delta$  ppm: 2.34 (s, 3H, CH<sub>3</sub>), 3.91-3.92 (s, magnetically different, 3H, OCH<sub>3</sub>), 3.93-3.98 (s, magnetically different 3H, OCH<sub>3</sub>), 7.11-8.31 (s, 11H, Ar-H);  $^{13}\text{C}$  NMR (DMSO- $d_6$ )  $\delta$  ppm: 22.62, 56.12, 56.41, 109.87, 110.67, 115.45, 125.83, 126.32, 128.29, 128.64, 128.75, 129.41, 130.68, 132.43, 138.12, 140.45, 146.89, 153.42, 154.87, 156.55, 163.12, 165.78, 169.76; HRMS (EI)  $m/z$  calcd for C<sub>25</sub>H<sub>20</sub>N<sub>4</sub>O<sub>4</sub>: 440.1485; found: 441.1489.

**6.2.10 3-(5-benzyl-1,3,4-oxadiazol-2-yl)-6,7-dimethoxy-2-phenylquinazolin-4(3H)-one (29)**

This compound was prepared and purified as per the above mentioned procedure: yield 62 %; mp 288-291 °C. IR (KBr,  $\nu_{\text{max}}$ ,  $\text{cm}^{-1}$ ): 2982.23 (Ar-CH), 2918.28 (Ali-CH) 1644.88 (C=O), 1561.23 (C=N);  $^1\text{H}$  NMR (DMSO- $d_6$ )  $\delta$  ppm: 2.75 (s, 2H, CH<sub>2</sub>), 3.91-3.92 (s, magnetically different, 3H, OCH<sub>3</sub>), 3.93-3.98 (s, magnetically different 3H, OCH<sub>3</sub>) 7.09-8.19 (s, 12H, Ar-H).  $^{13}\text{C}$  NMR (DMSO- $d_6$ )  $\delta$  ppm: 30.51, 56.12, 56.41, 108.87, 109.46, 116.76, 126.13, 128.47, 128.67, 128.82, 129.97, 130.46, 132.47, 136.53, 145.73, 153.24, 155.46, 158.26, 163.32, 167.42, 168.12; HRMS (EI)  $m/z$  calcd for C<sub>25</sub>H<sub>20</sub>N<sub>4</sub>O<sub>4</sub>: 440.1485; found: 440.1481.

**6.2.11 6,7-dimethoxy-2-phenyl-3-(5-(pyridin-3-yl)-1,3,4-oxadiazol-2-yl)quinazolin-4(3H)-one (34)**

This compound was prepared and purified as per the above mentioned procedure: yield 62 %; mp 288-291 °C. IR (KBr,  $\nu_{\text{max}}$ ,  $\text{cm}^{-1}$ ): 2924.18 (CH), 1641.12 (C=O), 1542.87 (C=N);  $^1\text{H}$  NMR (DMSO- $d_6$ )  $\delta$  ppm: 3.91-3.92 (s, magnetically different, 3H, OCH<sub>3</sub>), 3.93-3.98 (s, magnetically different 3H, OCH<sub>3</sub>) 7.14-8.23 (m, 11H, Ar-H);  $^{13}\text{C}$  NMR (DMSO- $d_6$ )  $\delta$  ppm: 56.12, 56.41, 108.74, 110.13, 115.54, 124.78, 125.46, 128.63, 128.78, 128.84, 130.64, 134.56, 144.56, 148.45, 153.43, 154.13, 155.62, 156.76, 163.53, 164.94, 168.73; HRMS (EI)  $m/z$  calcd for C<sub>23</sub>H<sub>17</sub>N<sub>5</sub>O<sub>4</sub>: 427.1281; found: 427.1285.

**6.2.12 6,7-dimethoxy-3-(5-(4-methoxyphenyl)-1,3,4-oxadiazol-2-yl)-2-phenylquinazolin-4(3H)-one (40)**

This compound was prepared and purified as per the above mentioned procedure: yield 62 %; mp 288-291 °C. IR (KBr,  $\nu_{\text{max}}$ ,  $\text{cm}^{-1}$ ): 2920.32 (CH), 1647.26 (C=O), 1534.78 (C=N);  $^1\text{H}$  NMR (DMSO- $d_6$ )  $\delta$  ppm: 3.91-3.92 (s, magnetically different, 3H, OCH<sub>3</sub>), 3.93-3.98 (s, magnetically different 3H, OCH<sub>3</sub>), 3.89 (s, 3H, OCH<sub>3</sub>), 6.84-8.09 (m, 11H, Ar-H);  $^{13}\text{C}$  NMR (DMSO- $d_6$ )  $\delta$  ppm: 55.62, 56.12, 56.41, 108.56, 109.83, 116.65, 117.74, 117.94, 118.42, 128.22, 128.46, 128.78, 132.41, 145.67, 153.11, 154.34, 158.27, 163.76, 164.76, 166.35, 168.13; HRMS (EI)  $m/z$  calcd for C<sub>25</sub>H<sub>20</sub>N<sub>4</sub>O<sub>5</sub>: 456.1434; found: 456.1438.

**6.2.13 3-(5-(4-chlorobenzyl)-1,3,4-oxadiazol-2-yl)-6,7-dimethoxy-2-phenylquinazolin-4(3H)-one (41)**

This compound was prepared and purified as per the above mentioned procedure: yield 62 %; mp 288-291 °C. IR (KBr,  $\nu_{\text{max}}$ ,  $\text{cm}^{-1}$ ): 2991.69 (Ar-CH), 2865.45 (Ali-CH), 1642.74 (C=O), 1541.86 (C=N), 768.66 (C-Cl);  $^1\text{H}$  NMR (DMSO- $d_6$ )  $\delta$  ppm: 2.94 (s, 2H, CH<sub>2</sub>), 3.91-3.92 (s, magnetically different, 3H, OCH<sub>3</sub>), 3.93-3.98 (s, magnetically different 3H, OCH<sub>3</sub>) 7.04-8.29 (m, 11H, Ar-H);  $^{13}\text{C}$  NMR (DMSO- $d_6$ )  $\delta$  ppm: 30.45, 56.12, 56.41, 108.57, 109.77, 116.31, 126.27, 128.36, 128.67, 128.82, 130.81, 131.43, 132.49, 134.53, 148.67, 153.24, 154.54, 156.52, 163.56, 166.64, 168.33; HRMS (EI)  $m/z$  calcd for C<sub>25</sub>H<sub>19</sub>ClN<sub>4</sub>O<sub>4</sub>: 474.1095; found: 474.1091.

**6.2.14 6,7-dimethoxy-2-phenyl-3-(5-phenyl-1,3,4-thiadiazol-2-yl)quinazolin-4(3H)-one (45)**

This compound was prepared and purified as per the above mentioned procedure: yield 62 %; mp 288-291 °C. IR (KBr,  $\nu_{\max}$ ,  $\text{cm}^{-1}$ ): 2924.18 (CH), 1639.55 (C=O), 1552.34 (C=N);  $^1\text{H}$  NMR (DMSO- $d_6$ )  $\delta$  ppm: 3.91-3.92 (s, magnetically different, 3H, OCH<sub>3</sub>), 3.93-3.98 (s, magnetically different 3H, OCH<sub>3</sub>) 7.21-8.44 (m, 12H, Ar-H);  $^{13}\text{C}$  NMR (DMSO- $d_6$ )  $\delta$  ppm: 56.12, 56.41, 108.67, 110.47, 116.41, 124.25, 126.46, 128.76, 128.88, 130.42, 132.71, 134.79, 136.55, 144.75, 153.26, 154.47, 156.29, 163.76, 172.78, 174.13; HRMS (EI)  $m/z$  calcd for C<sub>24</sub>H<sub>18</sub>N<sub>4</sub>O<sub>3</sub>S: 442.1100; found: 443.1104.

**6.2.15 6,7-dimethoxy-3-(5-methyl-1,3,4-thiadiazol-2-yl)-2-phenylquinazolin-4(3H)-one (46)**

This compound was prepared and purified as per the above mentioned procedure: yield 62 %; mp 288-291 °C. IR (KBr,  $\nu_{\max}$ ,  $\text{cm}^{-1}$ ): 2924.35 (Ar-CH), 2835.09 (Ali-CH), 1677.82 (C=O), 1541.32 (C=N);  $^1\text{H}$  NMR (DMSO- $d_6$ )  $\delta$  ppm: 2.54 (s, 3H, CH<sub>3</sub>), 3.91-3.92 (s, magnetically different, 3H, OCH<sub>3</sub>), 3.93-3.98 (s, magnetically different 3H, OCH<sub>3</sub>) 7.02-8.09 (m, 11H, Ar-H).  $^{13}\text{C}$  NMR (DMSO- $d_6$ )  $\delta$  ppm: 19.78, 56.12, 56.41, 108.75, 109.75, 116.31, 128.22, 128.46, 128.58, 130.31, 140.27, 145.57, 153.21, 154.54, 156.72, 163.76, 172.47; HRMS (EI)  $m/z$  calcd for C<sub>19</sub>H<sub>16</sub>N<sub>4</sub>O<sub>3</sub>S: 380.0943; found: 380.0948.

**6.2.16 3-(5-(4-chlorophenyl)-1,3,4-thiadiazol-2-yl)-6,7-dimethoxy-2-phenylquinazolin-4(3H)-one (47)**

This compound was prepared and purified as per the above mentioned procedure: yield 62 %; mp 288-291 °C. IR (KBr,  $\nu_{\max}$ ,  $\text{cm}^{-1}$ ): 2924.18 (CH), 1673.30 (C=O), 1538.23 (C=N), 766.83 (C-Cl).  $^1\text{H}$  NMR (DMSO- $d_6$ )  $\delta$  ppm: 3.91-3.92 (s, magnetically different, 3H, OCH<sub>3</sub>), 3.93-3.98 (s, magnetically different 3H, OCH<sub>3</sub>) 7.18-8.42 (m, 11H, Ar-H);  $^{13}\text{C}$  NMR (DMSO- $d_6$ )  $\delta$  ppm: 56.12, 56.41, 108.87, 110.37, 116.14, 126.24, 128.36, 128.58, 128.69, 129.73, 130.81, 132.86, 136.83, 144.87, 153.21, 153.54, 156.92, 160.36, 173.74, 174.23; HRMS (EI)  $m/z$  calcd for C<sub>24</sub>H<sub>17</sub>ClN<sub>4</sub>O<sub>3</sub>S: 476.0710; found: 478.0715.

**6.2.17 3-(5-cyclopropyl-1,3,4-thiadiazol-2-yl)-6,7-dimethoxy-2-phenylquinazolin-4(3H)-one (50)**

This compound was prepared and purified as per the above mentioned procedure: yield 62 %; mp 288-291 °C. IR (KBr,  $\nu_{\max}$ ,  $\text{cm}^{-1}$ ): 2925.99 (Ar-CH), 2851.55 (Ali-CH), 1641.73 (C=O), 1532.34 (C=N);  $^1\text{H}$  NMR (DMSO- $d_6$ )  $\delta$  ppm: 1.50-2.43 (m, 5H, cyclopropyl), 3.91-3.92 (s, magnetically different, 3H, OCH<sub>3</sub>), 3.93-3.98 (s, magnetically different 3H, OCH<sub>3</sub>) 6.75-8.01 (m, 11H, Ar-H);  $^{13}\text{C}$  NMR (DMSO- $d_6$ )  $\delta$  ppm: 8.14, 9.35, 56.12, 56.41, 108.75, 110.73, 116.31, 128.38, 128.55, 128.69, 130.51, 144.57, 153.61, 154.78, 156.42, 163.76, 168.84, 172.48; HRMS (EI)  $m/z$  calcd for C<sub>21</sub>H<sub>18</sub>N<sub>4</sub>O<sub>3</sub>S: 406.1100; found: 406.1106.

**6.2.18 N-(5-(6,7-dimethoxy-4-oxo-2-phenylquinazolin-3(4H)-yl)-1,3,4-thiadiazol-2-yl) benzamide (51)**

This compound was prepared and purified as per the above mentioned procedure: yield 62 %; mp 288-291 °C. IR (KBr,  $\nu_{\max}$ ,  $\text{cm}^{-1}$ ): 3212.34 (NH), 2918.18 (CH), 1678.34 (C=O), 1563.32 (C=N);  $^1\text{H}$  NMR (DMSO- $d_6$ )  $\delta$  ppm: 3.91-3.92 (s, magnetically different, 3H, OCH<sub>3</sub>), 3.93-3.98 (s, magnetically different 3H, OCH<sub>3</sub>) 6.65-7.88 (m, 12H, Ar-H), 9.12 (s, 1H, NH);  $^{13}\text{C}$  NMR (DMSO- $d_6$ )  $\delta$  ppm: 56.12, 56.41, 108.47, 109.75, 116.15, 126.59, 128.26, 128.56, 128.74, 129.84, 130.14, 132.81, 134.42, 144.73, 150.83, 152.13, 153.44, 156.92, 163.64, 165.87, 172.64; HRMS (EI)  $m/z$  calcd for C<sub>25</sub>H<sub>19</sub>N<sub>5</sub>O<sub>4</sub>S: 485.1158; found: 485.1162.

**6.2.19 3-(5-benzyl-1,3,4-thiadiazol-2-yl)-6,7-dimethoxy-2-phenylquinazolin-4(3H)-one (55)**

This compound was prepared and purified as per the above mentioned procedure: yield 62 %; mp 288-291 °C. IR (KBr,  $\nu_{\max}$ ,  $\text{cm}^{-1}$ ): 2925.15 (Ar-CH), 2901.24 (Ali-CH), 1652.48 (C=O), 1563.46 (C=N);  $^1\text{H}$  NMR (DMSO- $d_6$ )  $\delta$  ppm: 2.53 (s, 3H, CH<sub>2</sub>), 3.91-3.92 (s,

magnetically different 3H, OCH<sub>3</sub>), 3.93-3.98 (s, magnetically different 3H, OCH<sub>3</sub>) 7.21-8.41 (s, 12H, Ar-H); <sup>13</sup>C NMR (DMSO-d<sub>6</sub>) δ ppm: 33.62, 56.12, 56.41, 108.57, 109.37, 116.51, 124.67, 128.46, 128.55, 128.77, 128.82, 129.34, 130.15, 134.52, 142.57, 153.23, 154.44, 158.23, 163.45, 164.23, 172.43; HRMS (EI) m/z calcd for C<sub>25</sub>H<sub>20</sub>N<sub>4</sub>O<sub>3</sub>S: 456.1256; found: 458.1260.

#### 6.2.20 6,7-dimethoxy-2-phenyl-3-(5-(pyridin-3-yl)-1,3,4-thiadiazol-2-yl)quinazolin-4(3H)-one (63)

This compound was prepared and purified as per the above mentioned procedure: yield 62 %; mp 288-291 °C. IR (KBr, ν<sub>max</sub>, cm<sup>-1</sup>): 2996.16 (CH), 1645.09 (C=O), 1561.34 (C=N); <sup>1</sup>H NMR (DMSO-d<sub>6</sub>) δ ppm: 3.91-3.92 (s, magnetically different, 3H, OCH<sub>3</sub>), 3.93-3.98 (s, magnetically different 3H, OCH<sub>3</sub>) 7.01-8.19 (m, 11H, Ar-H); <sup>13</sup>C NMR (DMSO-d<sub>6</sub>) δ ppm: 56.12, 56.41, 108.47, 110.75, 116.61, 126.23, 128.33, 128.45, 128.78, 130.51, 132.54, 134.53, 146.57, 148.59, 150.92, 153.25, 154.54, 156.52, 163.56, 173.34, 174.51; HRMS (EI) m/z calcd for C<sub>23</sub>H<sub>17</sub>N<sub>5</sub>O<sub>3</sub>S: 443.1052; found: 443.1056.

#### 6.2.21 6,7-dimethoxy-3-(5-(4-methoxyphenyl)-1,3,4-thiadiazol-2-yl)-2-phenylquinazolin-4(3H)-one (68)

This compound was prepared and purified as per the above mentioned procedure: yield 62 %; mp 288-291 °C. IR (KBr, ν<sub>max</sub>, cm<sup>-1</sup>): 2930.57 (CH), 1666.48 (C=O), 1564.78 (C=N); <sup>1</sup>H NMR (DMSO-d<sub>6</sub>) δ ppm: 3.91-3.92 (s, magnetically different, 3H, OCH<sub>3</sub>), 3.93-3.98 (s, magnetically different 3H, OCH<sub>3</sub>), 3.89 (s, 3H, OCH<sub>3</sub>), 6.78-8.12 (m, 11H, Ar-H); <sup>13</sup>C NMR (DMSO-d<sub>6</sub>) δ ppm: 55.08, 56.12, 56.41, 108.13, 110.13, 116.42, 118.31, 122.13, 128.23, 128.42, 128.67, 129.57, 130.15, 146.27, 152.15, 153.37, 154.54, 156.62, 162.26, 164.18, 172.37; HRMS (EI) m/z calcd for C<sub>25</sub>H<sub>20</sub>N<sub>4</sub>O<sub>4</sub>S: 472.1205; found: 472.1209

#### 6.2.22 3-(5-(4-chlorobenzyl)-1,3,4-thiadiazol-2-yl)-6,7-dimethoxy-2-phenylquinazolin-4(3H)-one (69)

This compound was prepared and purified as per the above mentioned procedure: yield 62 %; mp 288-291 °C. IR (KBr, ν<sub>max</sub>, cm<sup>-1</sup>): 2918.29 (Ar-CH), 2910.24 (Allyl-CH), 1664.14 (C=O), 1534.24 (C=N), 752.68 (C-Cl). <sup>1</sup>H NMR (DMSO-d<sub>6</sub>) δ ppm: 2.91 (s, 2H, CH<sub>2</sub>), 3.91-3.92 (s, magnetically different, 3H, OCH<sub>3</sub>), 3.93-3.98 (s, magnetically different 3H, OCH<sub>3</sub>) 7.02-8.28 (m, 11H, Ar-H); <sup>13</sup>C NMR (DMSO-d<sub>6</sub>) δ ppm: 34.26, 56.12, 56.41, 108.37, 110.74, 116.31, 128.23, 128.46, 128.67, 128.83, 130.41, 132.82, 133.59, 134.35, 146.73, 153.41, 154.54, 156.25, 163.56, 164.34, 172.23; HRMS (EI) m/z calcd for C<sub>25</sub>H<sub>19</sub>ClN<sub>4</sub>O<sub>3</sub>S: 490.0866; found: 490.0871.

### 6.3 In vitro VEGFR-2 kinase assay and HUVEC Cell Assay <sup>31</sup>

HTRF assays are homogeneous time-resolved assays that generate a signal by FRET between donor and acceptor molecules. When formatted for kinase assays, the Eu-cryptate is usually conjugated to a phospho-specific antibody and is presented upon binding of the antibody to the phosphorylated product, while the streptavidin-conjugated allophycocyanin binds to the biotin on the substrate to complete the detection complex. When the two entities get close proximity, energy transfer occurs upon excitation and APC emits a specific long-lived fluorescence at 665 nm. The kinases were purified as the intracellular domain of human VEGFR-2 fused by GST. The catalytic activity of the kinase was detected by using a biotinylated synthetic peptide as a substrate, biotin-aminohexyl-EEEEYFELVAKKKK-NH<sub>2</sub>, for VEGFR-2. Phosphorylated substrate is measured by streptavidin linked-APC and europium-labeled anti-phosphorylated tyrosine antibody. Briefly, the assay method is as follows: the working solution (100 nM TK-substrate, 3 μg/ml GSTVEGFR-2, 100 nM ATP, 1 mM DTT, 1 mM MnCl<sub>2</sub>, 1 mM MgCl<sub>2</sub> and 20 nM SEB in 10 μl reaction volume) is incubated at 37 °C for 30 min; the detection solution (6.25 nM Streptavidin-XL665, 5 μl/well TK antibody-cryptate) is added to stop the reaction, and placed at room temperature for 30 min for determination (excitation at 310 nm, emission at 665 nm/ 620 nm).



## ARTICLE

RSC Advances

Cell assay: HUVEC were developed in M199 containing 10% FBS and kanamycin ( $50 \mu\text{mL}^{-1}$ ) in a humidified 5%  $\text{CO}_2$  incubator at 37 °C. After the cells had grown to confluence, they were disaggregated in trypsin solution, washed with M199 containing 10% FBS, centrifuged at 125 g for 5 min, re-suspended and then subcultured in accordance to standard protocols. Cells from passages 4-8 were used. HUVEC proliferation in the presence of growth factors was evaluated using Sulforhodamine B (SRB) assay. In brief, HUVEC were plated in 96-well plates (1000 cells/well) and dosed with tested compound + VEGF (15 ng/ml). The cultures were incubated for 48 h (37 °C; 5%  $\text{CO}_2$ ) followed by addition of SRB and finally, reincubated for 15 min. Cells were harvested and assayed using a ELISA counter with reading at 490 nm.  $\text{IC}_{50}$  data was interpolated as described above.

**Acknowledgement**

The authors would like to thank National Research Foundation, South Africa and College of Health Sciences, University of KwaZulu-Natal, South Africa for funding this project.

## References

- 1 Yang, Y.; Shi, L.; Zhou, Y.; Li, H.-Q.; Zhu, Z.-W.; Zhu, H. L. Design, synthesis and biological evaluation of quinoline amide derivatives as novel VEGFR-2 inhibitors. *Bioorg. Med. Chem. Lett.* 2010, 20, 6653-6656
- 2 (a) Harris, P. A.; Bolor, A.; Cheung, M.; Kumar, R.; Crosby, R. M.; Davis-Ward, R. G.; Epperly, A. H.; Hinkle, K. W.; Hunter, R. N.; Johnson, J. H.; Knick, V. B.; Laudeman, C. P.; Luttrell, D. K.; Mook, R. A.; Nolte, R. T.; Rudolph, S. K.; Szewczyk, J. R.; Truesdale, A. T.; Veal, J. M.; Wang, L. P.; Stafford, J. A. Discovery of 5-[[4-[(2,3-dimethyl-2H-indazol-6-yl)methylamino]-2-pyrimidinyl]amino]-2-methyl-benzenesulfonamide (pazopanib), a novel and potent vascular endothelial growth factor receptor inhibitor. *J. Med. Chem.* 2008, 51, 4632-4640. (b) Rizvi, S.U.F.; Siddiqui, H.L.; Nisar, M.; Khan, N.; Khan, I. Discovery and molecular docking of quinolyl-thienyl chalcones as anti-angiogenic agents targeting VEGFR-2 tyrosine kinase. *Bioorg. Med. Chem. Lett.* 2012, 22, 942-944.
- 3 (a) Ferrara, N. VEGF and the quest for tumour angiogenesis factors. *Nat. Rev. Cancer* 2002, 2, 795-803. (b) Ferrara, N.; Gerber, H. P.; LeCouter, J. The biology of VEGF and its receptors. *Nat. Med.* 2003, 9, 669-676.
- 4 Ferrara, N. Vascular endothelial growth factor: basic science and clinical progress. *Endocr. Rev.* 2004, 25, 581-611.
- 5 Cook, K. M.; Figg, W. D. Angiogenesis inhibitors: current strategies and future prospects. *Cancer J. Clin.* 2010, 60, 222-243.
- 6 Weis, S. M.; Cheresh, D. A. Tumor angiogenesis: molecular pathways and therapeutic targets. *Nat. Med.* 2011, 17, 1359-1370.
- 7 Qi, F.; Li, A.; Inagaki, Y.; Kokudo, N.; Tamura, S.; Nakata, M. Antitumor activity of extracts and compounds from the skin of the toad *Bufo bufo gargarizans* Cantor. *Int. Immunopharmacol.* 2011, 11, 342-349.
- 8 Cruz, J. S.; Matsuda, H. Depressive effects of arenobufagin on the delayed rectifier K<sup>+</sup> current of guinea-pig cardiac myocytes. *Eur. J. Pharmacol.* 1994, 266, 317-325.
- 9 Cruz, J. S.; Matsuda, H. Arenobufagin, a compound in toad venom, blocks Na<sup>+</sup>,-K<sup>+</sup> pump current in cardiac myocytes. *Eur. J. Pharmacol.* 1993, 239, 223-226.
- 10 Cao, H.; Zhang, D.; Liu, J.; Hou, C.; Kurihara, H.; Ye, W. Inhibitory effect of arenobufagin on the adhesion, invasion and migration of human hepatoma carcinoma cells. *Chin. Pharm. Bull.* 2011, 27, 19-23.
- 11 Baudin, B.; Bruneel, A.; Bosselut, N.; Vaubourdolle, M. A protocol for isolation and culture of human umbilical vein endothelial cells. *Nat. Protoc.* 2007, 2, 481-485.
- 12 Corrigan, C. J.; Wang, W.; Meng, Q.; Fang, C.; Wu, H.; Reay, V. T-helper cell type 2 (Th2) memory T cell-potentiating cytokine IL-25 has the potential to promote angiogenesis in asthma. *Proc. Natl. Acad. Sci. USA* 2011, 108, 1579-1584.
- 13 Harris, P.A.; Harris, P. A.; Cheung, M.; Brown, M. L.; Veal, J. M.; Nolte, R.T.; Wang, L.; Liu, W.; Crosby, R. M.; Johnson, J. H.; Epperly, A. H.; Kumar, R.; Luttrell, D. K.; Stafford, J. A. Discovery and evaluation of 2-anilino-5-aryloxazoles as a novel class of VEGFR2 kinase inhibitors. *J. Med. Chem.* 2005, 48, 1610-1619.
- 14 Phase, version 3.1, Schrödinger, LLC, New York, NY, 2009, 7.
- 15 Dixon, S. L.; Smondyrev, A. M.; Knoll, E. H.; Rao, S. N.; Shaw, D. E.; Friesner, R. A. PHASE: a new engine for pharmacophore perception, 3D QSAR model development, and 3D database screening: 1. Methodology and preliminary results. *J. Comput. Aided Mol. Des.* 2006, 20, 647-671.

- 16 MacroModel, version 9.7, Schrödinger, LLC, New York, NY, 2009,11.
- 17 LigPrep, version 2.3, Schrödinger, LLC, New York, NY, 2009,12.
- 18 (a) Regina, G. L.; Silvestri, R.; Artico, M.; Lavecchia, A.; Novellino, E.; Befani, O.; Turini, P. New pyrrole inhibitors of monoamine oxidase: synthesis, biological evaluation, and structural determinants of MAO-A and MAO-B selectivity. *J. Med. Chem.*2007, 50, 922-931.(b) Shivakumar, D.; Williams, J.; Wu, Y. Prediction of absolute solvation free energies using molecular dynamics free energy perturbation and the OPLS force field. *J. Chem. Theory Comput.* 2010, 6, 1509-1519. (c) Jorgensen, W. L.; Maxwell, D. S.; Tirado-Rives, J., et al., Development and testing of the OPLS all-atom force field on conformational energetics and properties of organic liquids. *J. Am. Chem. Soc.* 1996, 118, 11225-11236. (d) Jorgensen, W. L.; Tirado-Rives, J. The OPLS [optimized potentials for liquid simulations] potential functions for proteins, energy minimizations for crystals of cyclic peptides and crambin. *J. Am. Chem. Soc.* 1988, 110, 1657-1666.
- 19 (a) Halgren, T. A.; Murphy, R. B.; Friesner, R. A.; Beard, H. S.; Frye, L. L.; Pollard, W. T.; Banks, J. L. Glide: a new approach for rapid, accurate docking and scoring. 2. Enrichment factors in database screening.*J. Med. Chem.*2004, 47, 1750-1759. (b) Friesner, R. A.; Banks, J. L.; Murphy, R. B.; Halgren, T. A.; Klicic, J. J.; Mainz, D. T.; Repasky, M. P.; Knoll, E. H.;Shelley, M.; Perry, J. K.; Shaw, D. E.; Francis, P.; P.S. Shenkin, Glide: A new approach for rapid, accurate docking and scoring. 1. method and assessment of docking accuracy. *J. Med. Chem.*2004, 47, 1739-1749. (c) Sherman, W.; Day, T.; Jacobson, M. P.; Friesner, R. A.; Farid, R. Novel Procedure for Modeling Ligand/Receptor Induced Fit Effects. *J. Med. Chem.*2006, 49, 534-553.
- 20 <http://www.rcsb.org/pdb/explore/explore.3B8Q>.
- 21 Schrödinger Suite 2009 Protein Preparation Wizard; Epik version 2.0; Impact version 5.5. Schrödinger, LLC, New York, NY, 2009, 14.
- 22 Antonio, G.; Amaury, F.; Severine R.; Amelie, L.; Perrine, S.; Philippe, C.; Laurence, G.; Patrick D. Synthesis and Structure-Activity Relationships of (Aryloxy) quinazoline Ureas as Novel, Potent, and Selective Vascular Endothelial Growth Factor Receptor-2 Inhibitors. *J. of Med. Chem.*2012, 55, 1189-1204.
- 23 (a) Friesner, R.A.; Banks, J.L.; Murphy, R.B.; Halgren, T.A.; Klicic, J.J.; Mainz, D.T.; Repasky, M.P.; Knoll, E.H.; Shelley, M.; Perry, J.K.; Shaw, D.E.; Francis, P.; Shenkin, P.S. Glide: A New Approach for Rapid, Accurate Docking and Scoring. 1. Method and Assessment of Docking Accuracy. *J. Med. Chem.*2004, 47, 1739-1749. (b) Sherman, W.; Day, T.; Jacobson, M.P.; Friesner, R.A.; Farid, R. Novel Procedure for Modeling Ligand/Receptor Induced Fit Effects. *J. Med. Chem.*2006, 49, 534-553. (c) Narkhede, S.S.; Degani, M.S. Pharmacophore Refinement and 3D-QSAR Studies of Histamine H3 Antagonists. *QSAR Comb. Sci.*2007, 26, 744-753. (d) Tawari, N.R.; Bag, S.; Degani, M.S. Pharmacophore mapping of a series of pyrrolopyrimidines, indolopyrimidines and their congeners as multidrug resistance-associated protein (MRP1) modulators. *J. Mol. Model.*2008, 14, 911-921. (e) Golbraikh, A.; Shen, M.; Xiao, Z.; Xiao, Y.D.; Lee, K.H.; Tropsha, A. Rational selection of training and test sets for the development of validated QSAR models. *J. Comput. Aided Mol. Des.*2003, 17, 241-253.
- 24 Zhong, H.; Tran, L.M.; Jenna, L. Induced-fit docking studies of the active and inactive states of protein tyrosine kinases. *J. Mol. Graph. Mod.*2009, 28, 336-346.

- 25 Combiglide 2.5 (2009) User manual. Schrodinger, New York.
- 26 QikProp, version 9.0, Schrodinger, LLC, New York, NY, 2010.
- 27 Ligprep, version 9.0, Schrodinger, LLC, New York, NY, 2010.
- 28 Lipinski, C.A.; Lombardo, F.; Dominy, B.W.; Feeney, P.J. Experimental and computational approaches to estimate solubility and permeability in drug discovery and development settings. *Adv. Drug Deliv. Rev.* 2001, 23, 3-26.
- 29 Krantz, A.; Spencer, R. W.; Tam, T.F.; Liak, T. J.; Copp, L. J. Design and synthesis of 4H-3,1-benzoxazin-4-ones as potent alternate substrate inhibitors of human leukocyte elastase. *J. Med. Chem.* 1990, 33, 464-479.
- 30 Zentmyer, D. T.; Wagner, E. C. The so-called acylanthranils (3,1,4-benzoxazones). I. Preparation; reactions with water, ammonia and aniline; structure. *J. Org. Chem.* 1949, 14, 967-981.
- 31 Yu, B.; Tang, L.; Li, Y.; Song, S. H.; Ji, X. L.; Lin, M. S.; Wu, C. F. Design, synthesis and antitumor activity of 4-aminoquinazoline derivatives targeting VEGFR-2 tyrosine kinase. *Bioorg. Med. Chem. Lett.* 2012, 22, 110-114.
- 32 Noolvi, M. N.; Patel, H. M. Synthesis and in vitro anti-tumor activity of substituted quinazoline and quinoxaline derivatives: search for anti-cancer agent. *Eur. J. Med. Chem.* 2011, 46, 2327-46.

**Table 1** Experimental and predicted activity of quinazoline derivatives used in training and test set for VEGFR-2 inhibition using Model-I

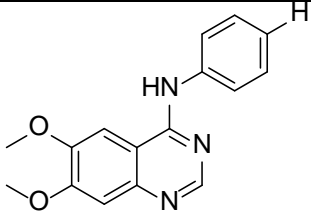
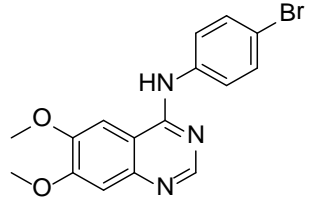
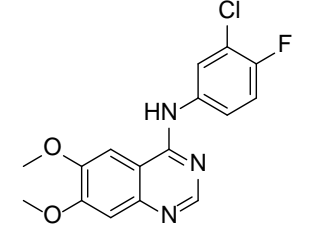
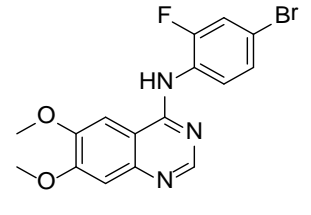
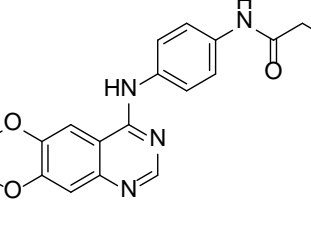
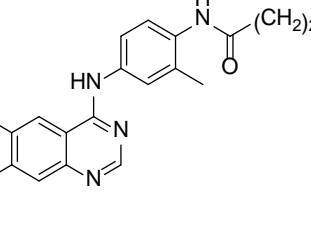
Sr. No	Compounds	IC <sub>50</sub> (nm)	pIC <sub>50</sub>		Residual
			Exp.	Pred.	
1 <sup>T</sup>		7.00	0.845	0.967	-0.122
2 <sup>T</sup>		0.80	0.097	0.108	-0.011
3 <sup>T</sup>		5.30	0.724	0.784	-0.060
4		1.65	0.217	0.315	-0.098
5 <sup>T</sup>		7.30	0.863	0.881	-0.018
6		4.0	0.845	0.967	-0.122

Table 1 Continue

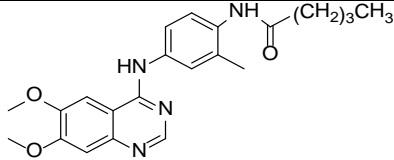
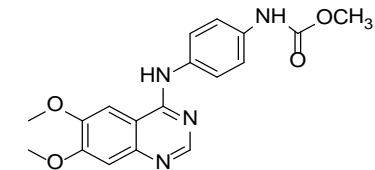
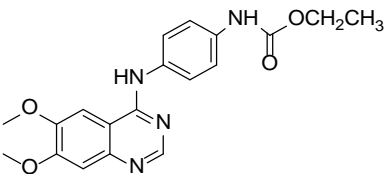
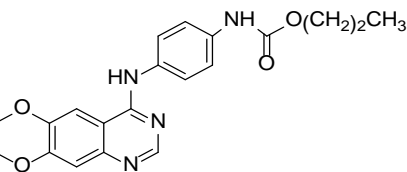
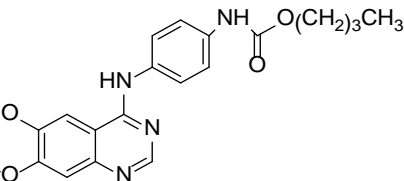
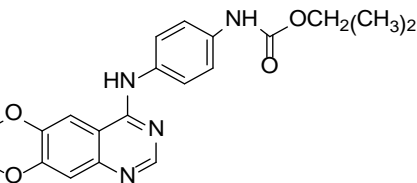
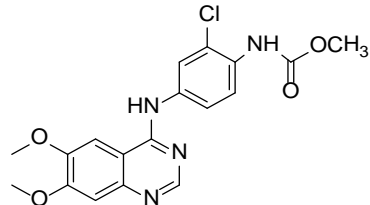
Sr. No	Compounds	IC <sub>50</sub> (nm)	pIC <sub>50</sub>		Residual
			Exp.	Pred.	
7 <sup>T</sup>		6.80	0.833	0.848	-0.015
8		5.80	0.763	0.810	-0.047
9		5.60	0.748	0.795	-0.047
10 <sup>T</sup>		5.00	0.699	0.781	-0.082
11 <sup>T</sup>		6.80	0.833	0.894	-0.061
12		5.05	0.703	0.835	-0.132
13		5.05	0.703	0.721	-0.018



Table 1 Continue

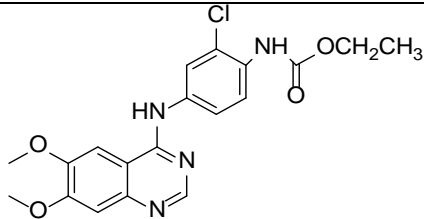
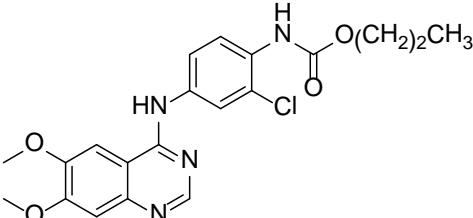
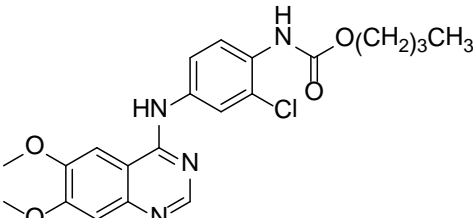
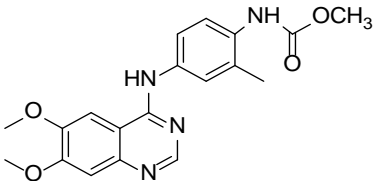
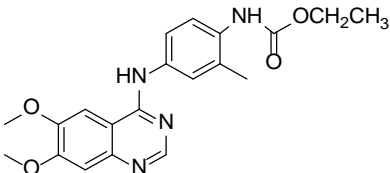
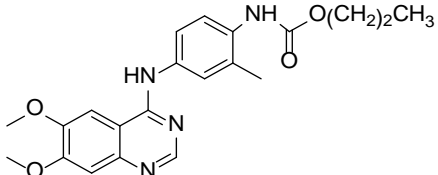
Sr. No	Compounds	IC <sub>50</sub> (nm)	pIC <sub>50</sub>		Residual
			Exp.	Pred.	
14 <sup>T</sup>		0.50	0.301	0.541	-0.240
15 <sup>T</sup>		3.30	0.519	0.712	-0.193
16 <sup>T</sup>		4.90	0.69	0.78	-0.009
17 <sup>T</sup>		0.85	0.071	0.084	-0.013
18		0.65	0.187	0.301	-0.118
19 <sup>T</sup>		0.85	0.071	0.097	-0.026

Table 1 Continue

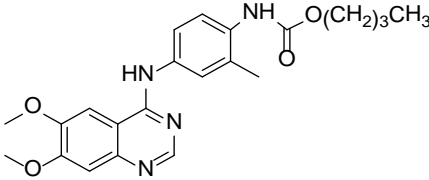
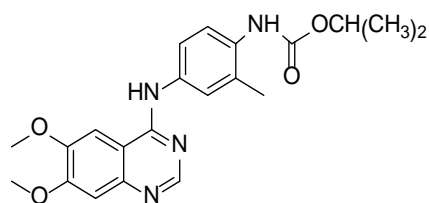
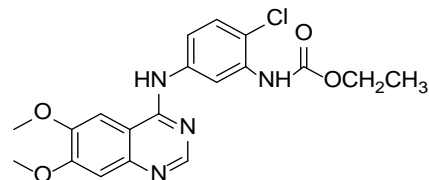
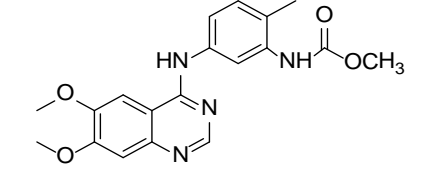
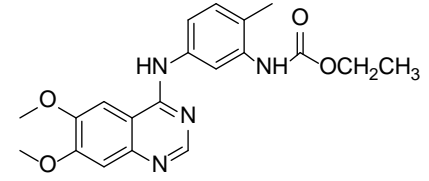
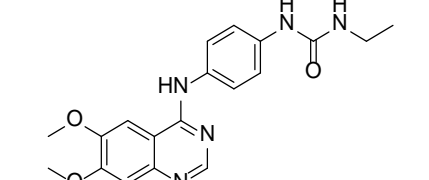
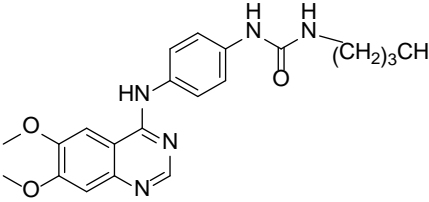
Sr. No	Compounds	IC <sub>50</sub> (nm)	pIC <sub>50</sub>		Residual
			Exp.	Pred.	
20 <sup>T</sup>		5.20	0.716	0.803	-0.087
21 <sup>T</sup>		5.25	0.72	0.75	-0.003
22 <sup>T</sup>		5.55	0.744	0.840	-0.096
23		7.80	0.892	0.961	-0.069
24 <sup>T</sup>		6.50	0.813	0.920	-0.107
25		4.65	0.667	0.811	-0.144
26 <sup>T</sup>		5.80	0.763	0.923	-0.160

Table 1 Continue

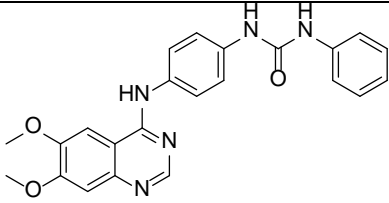
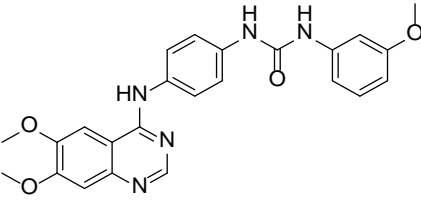
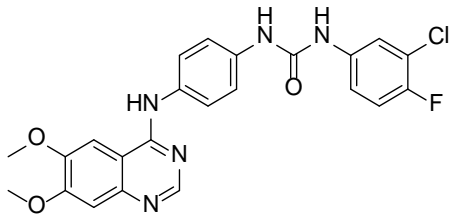
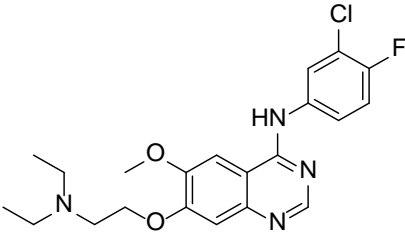
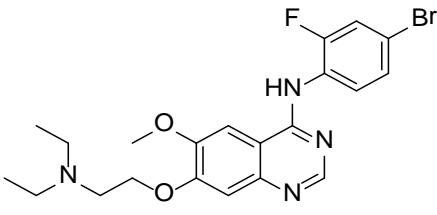
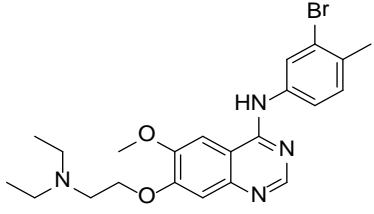
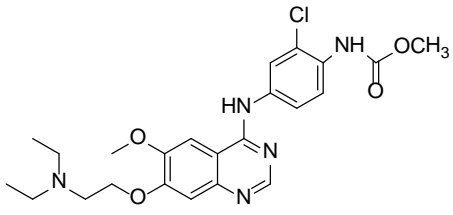
Sr. No	Compounds	IC <sub>50</sub> (nm)	pIC <sub>50</sub>		Residual
			Exp.	Pred.	
27 <sup>T</sup>		5.10	0.708	0.792	-0.084
28		6.20	0.792	0.857	-0.065
29 <sup>T</sup>		4.30	0.633	0.766	-0.133
30		6.90	0.839	0.965	-0.126
31 <sup>T</sup>		1.00	0	0.019	-0.019
32 <sup>T</sup>		6.45	0.81	0.94	-0.06
33 <sup>T</sup>		5.20	0.716	0.779	-0.063

Table 1 Continue

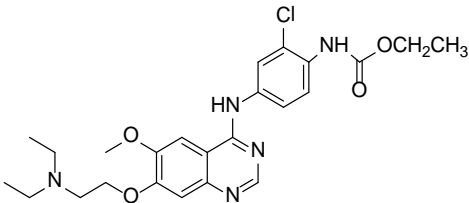
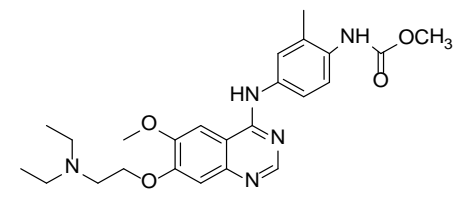
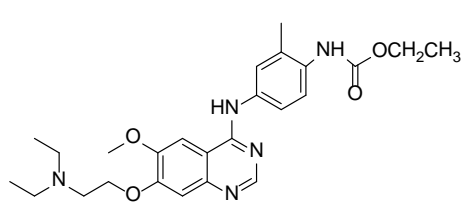
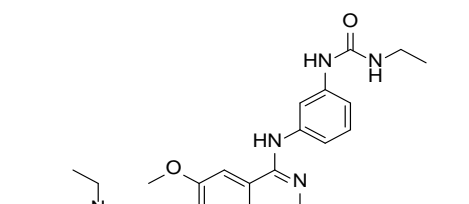
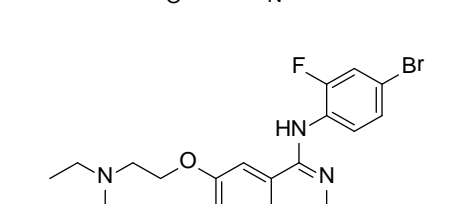
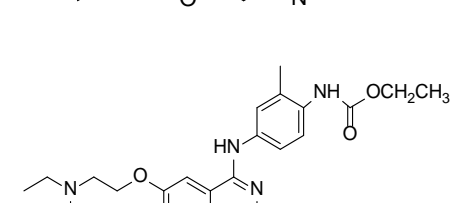
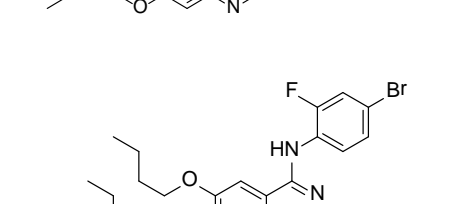
Sr. No	Compounds	IC <sub>50</sub> (nm)	pIC <sub>50</sub>		Residual
			Exp.	Pred.	
34		3.35	0.525	0.697	-0.172
35		6.95	0.842	0.732	-0.090
36 <sup>T</sup>		3.70	0.568	0.631	-0.063
37 <sup>T</sup>		6.60	0.82	0.90	-0.06
38 <sup>T</sup>		7.45	0.872	0.952	-0.080
39		7.25	0.86	1.08	-0.22
40 <sup>T</sup>		5.30	0.724	0.820	-0.096

Table 1 Continue

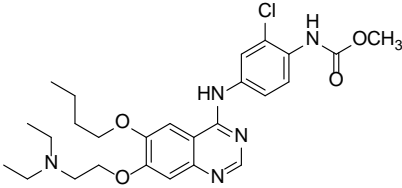
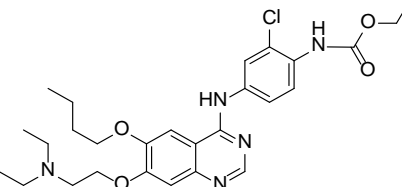
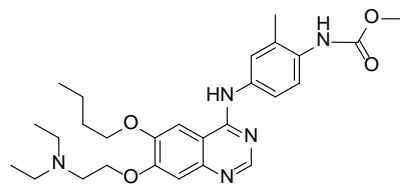
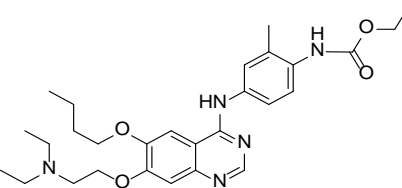
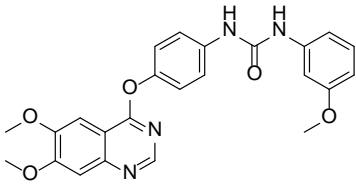
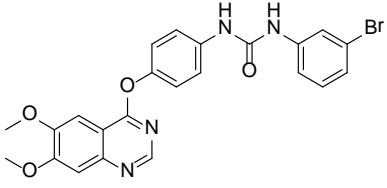
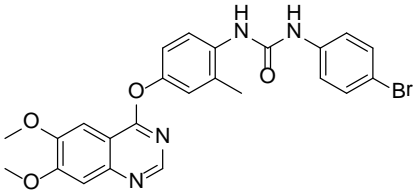
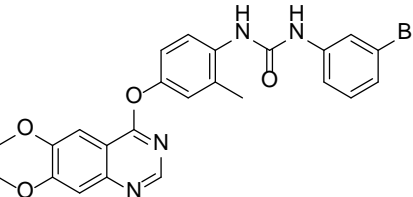
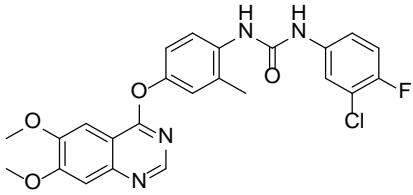
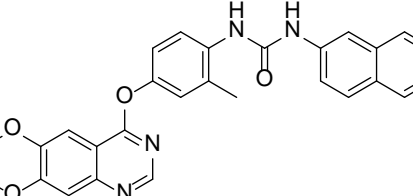
Sr. No	Compounds	IC <sub>50</sub> (nm)	pIC <sub>50</sub>		Residual
			Exp.	Pred.	
41 <sup>T</sup>		7.40	0.869	1.197	-0.328
42 <sup>T</sup>		4.80	0.681	0.817	-0.138
43 <sup>T</sup>		9.40	0.973	1.14	-0.167
44 <sup>T</sup>		5.70	0.756	0.856	-0.100
45 <sup>T</sup>		0.040	1.398	1.464	-0.066
46 <sup>T</sup>		0.006	2.222	2.291	-0.069

Table 1 Continue

Sr. No	Compounds	IC <sub>50</sub> (nm)	pIC <sub>50</sub>		Residual
			Exp.	Pred.	
47 <sup>T</sup>		0.040	1.398	1.571	-0.173
48		0.004	2.398	2.535	-0.137
49 <sup>T</sup>		0.006	2.222	2.420	-0.198
50 <sup>T</sup>		0.002	2.699	2.918	-0.219

Expt. = Experimental activity, Pred. = Predicted activity, T = Training Set



**Table 2** Statistical data for QSAR Models by PLS method for quinazoline derivatives.

Model	Hypothesis	Factor	SD	r <sup>2</sup>	F	Stability	RMSE	q <sup>2</sup>	Pearson R
Model-I	AAARR.8	5	0.1969	0.9687	148.6	0.8945	0.4487	0.7106	0.8709
Model-II	AAAHR.3	5	0.2156	0.9212	139.8	0.7723	0.4823	0.6867	0.8423
Model-III	AAHHR.7	5	0.2648	0.9045	129.9	0.7123	0.5234	0.6634	0.8276
Model-IV	AADHR.9	5	0.3585	0.8534	121.3	0.6987	0.5678	0.6432	0.7876
Model-V	AAADR.41	5	0.5881	0.8278	102.8	0.6824	0.5876	0.6023	0.7654
Model-VI	AAAAD.3	5	0.6445	0.8097	92.2	0.6542	0.6234	0.5723	0.7123
Model-VII	AADRR.10	5	0.6865	0.7856	90.6	0.5284	0.6532	0.5423	0.6452
Model-VIII	AADHR.16	5	0.7234	0.6434	79.4	0.2789	0.6856	0.5213	0.6128
Model-IX	AAADH.5	5	0.7457	0.5213	70.2	0.2553	0.7234	0.5129	0.5987
Model-X	ADHRR.34	5	0.8045	0.5045	48.1	0.2325	0.7324	0.4987	0.5862

Factor = Number of factors in the partial least squares regression model; SD = Standard deviation of the regression; r<sup>2</sup> = coefficient of determination; F = F test score; Stability = Stability of the model predictions to changes in the training set composition, maximum value is 1, this statistic can be used to compare models from different hypotheses; RMSE = Root-mean-square error; q<sup>2</sup> = cross validated r<sup>2</sup>; Pearson R = correlation between experimental and predicted activity for the test set.

**Table 3** Distances and angles of pharmacophore hypothesis by Model-I

Hypothesis	Site 1	Site 2	Distance (Å)	Hypothesis	Site 1	Site 2	Site 3	Angle	Hypothesis	Site 1	Site 2	Site 3	Angle	Hypothesis	Site 1	Site 2	Site 3	Angle
AAARR.8	A1	A3	5.0574	AAARR.8	A3	A4	A1	90.8	AAARR.8	A1	A3	R15	71	AAARR.8	A4	R13	R15	134.1
AAARR.8	A1	A4	4.856	AAARR.8	A3	A4	R13	61.6	AAARR.8	R13	A3	R15	70	AAARR.8	A3	R13	A1	178
AAARR.8	A1	R13	2.775	AAARR.8	A3	A4	R15	34.8	AAARR.8	A4	A1	A3	28.6	AAARR.8	A3	R13	R15	79.8
AAARR.8	A1	R15	6.425	AAARR.8	A1	A4	R13	29.2	AAARR.8	A4	A1	R13	29.5	AAARR.8	A1	R13	R15	102.1
AAARR.8	A3	A4	2.667	AAARR.8	A1	A4	R15	58.4	AAARR.8	A4	A1	R15	81.5	AAARR.8	A4	R15	A3	16.1
AAARR.8	A3	R13	2.800	AAARR.8	R13	A4	R15	30.3	AAARR.8	A3	A1	R13	1	AAARR.8	A4	R15	A1	40
AAARR.8	A3	R15	5.489	AAARR.8	A4	A3	A1	60.6	AAARR.8	A3	A1	R15	53.9	AAARR.8	A4	R15	R13	15.0
AAARR.8	A4	R13	2.798	AAARR.8	A4	A3	R13	61.5	AAARR.8	R13	A1	R15	52.9	AAARR.8	A3	R15	A1	55.1
AAARR.8	A4	R15	7.462	AAARR.8	A4	A3	R15	129.1	AAARR.8	A4	R13	A3	56.9	AAARR.8	A3	R15	R13	30.1
AAARR.8	R15	R13	5.24	AAARR.8	A1	A3	R13	1	AAARR.8	A4	R13	A1	121.2	AAARR.8	A1	R15	R13	25

Distances and angles between the pharmacophoric points (Site 1, 2 and 3) of hypothesis AAARR8 (refer Fig. 3)

**Table 4** Pharmacophoric alignment and predicted activity of designed compounds

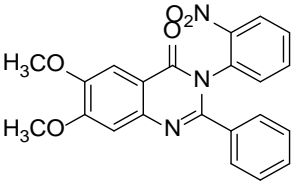

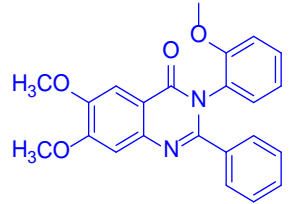
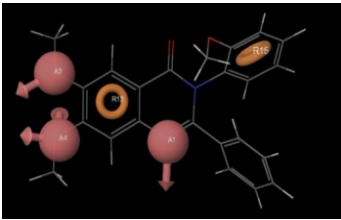
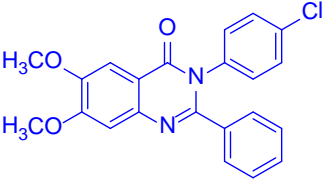
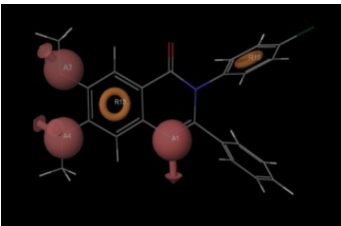
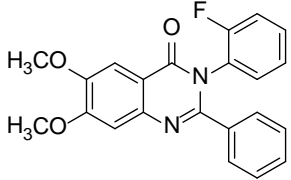
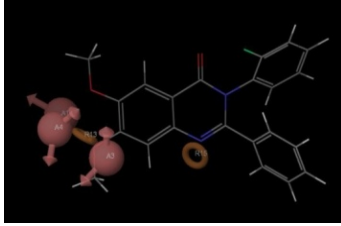
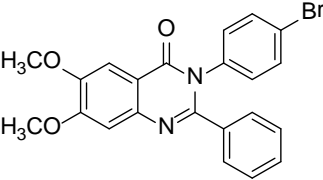
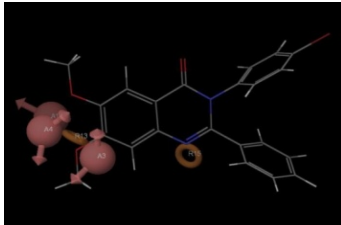
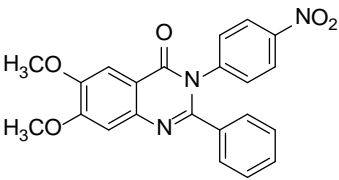
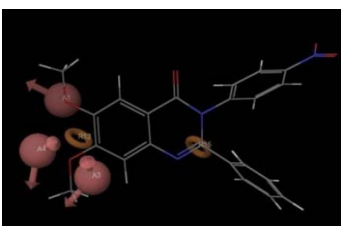
Code	Compounds	Pharmacophoric Fitness	Predicted Activity (IC <sub>50</sub> )
1			8.28
2			1.923
3			1.201
4			6.23
5			9.076
6			6.101

Table 4 Continue

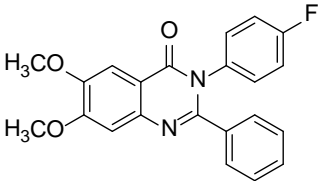
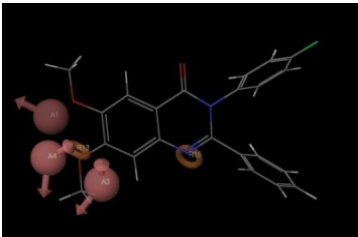
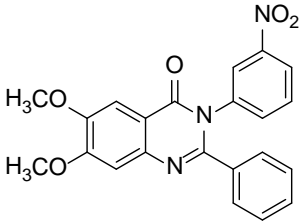
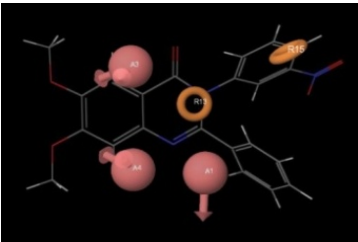
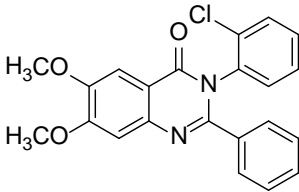
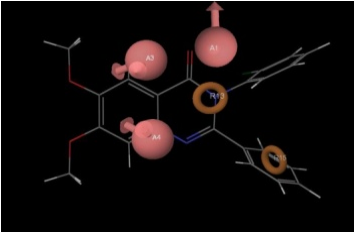
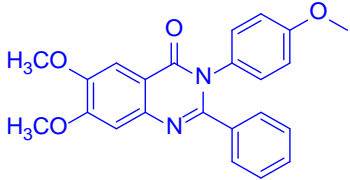
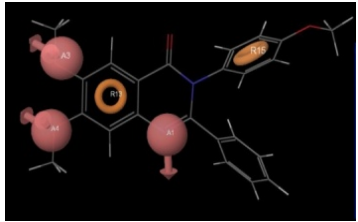
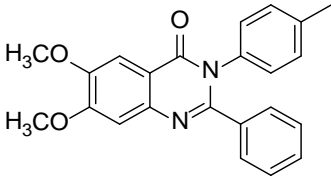
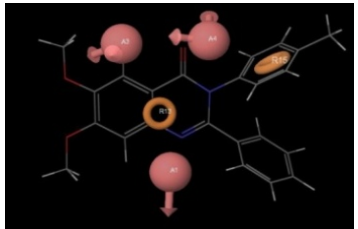
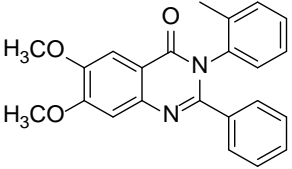
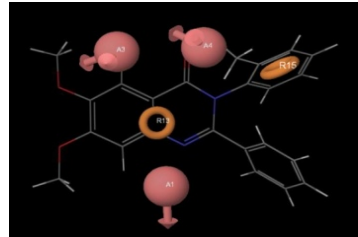
Code	Compounds	Pharmacophoric Fitness	Predicted Activity (IC <sub>50</sub> )
7			8.115
8			9.124
9			15.101
10			0.795
11			7.066
12			8.089

Table 4 Continue

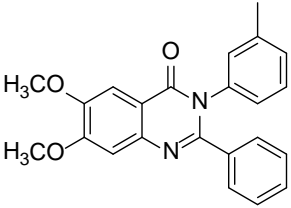
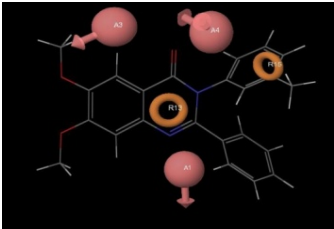
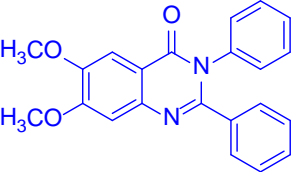
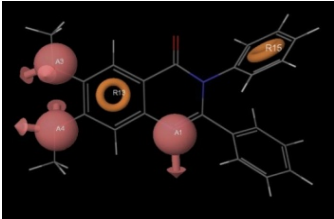
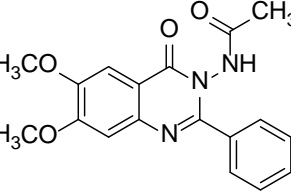
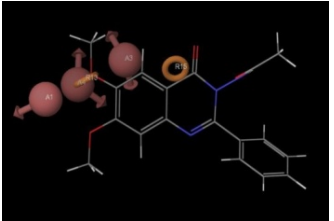
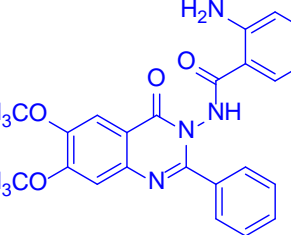
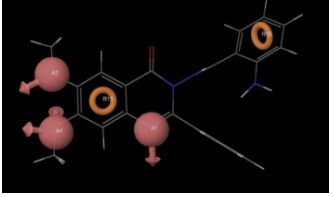
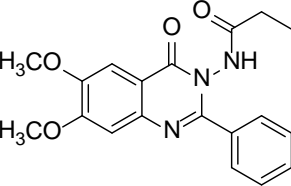
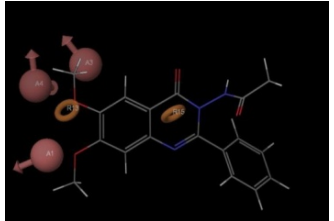
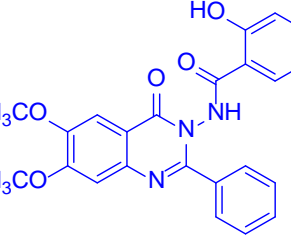
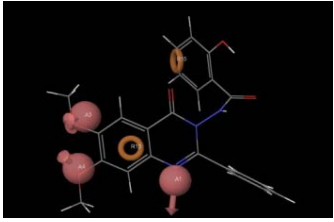
Code	Compounds	Pharmacophoric Fitness	Predicted Activity (IC <sub>50</sub> )
13			9.064
14			2.283
15			8.075
16			2.134
17			7.084
18			2.296

Table 4 Continue

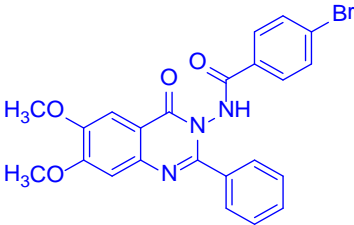
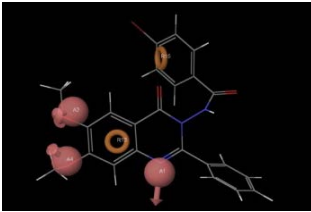
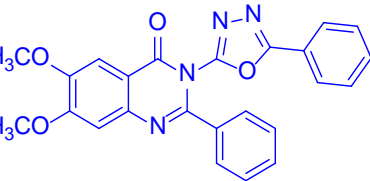
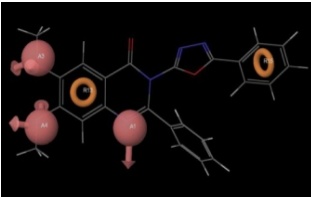
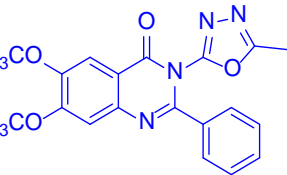
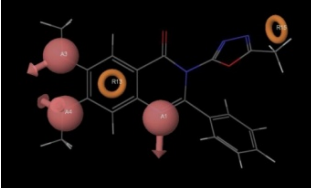

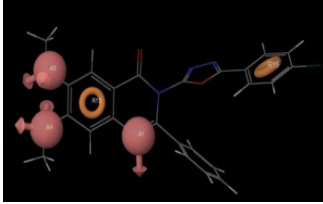
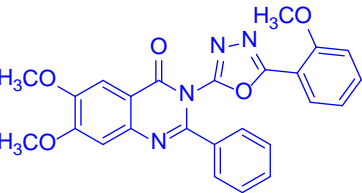
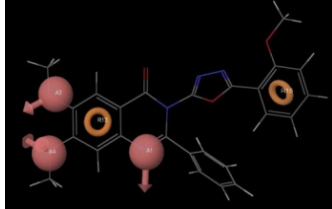
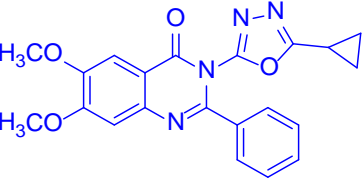
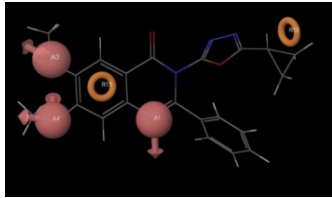
Code	Compounds	Pharmacophoric Fitness	Predicted Activity (IC <sub>50</sub> )
19			3.215
20			3.297
21			1.786
22			0.327
23			0.583
24			1.194

Table 4 Continue

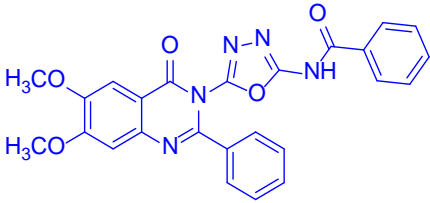
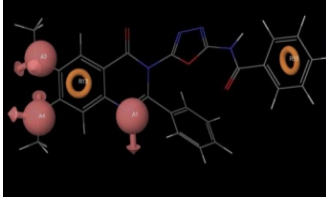
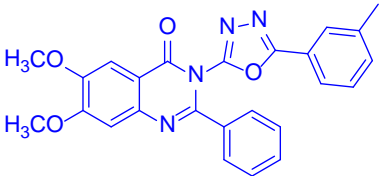
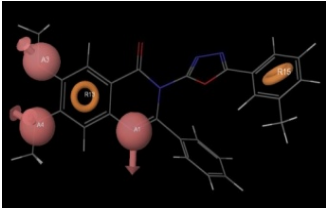
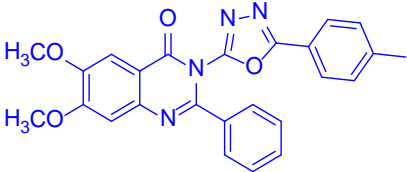
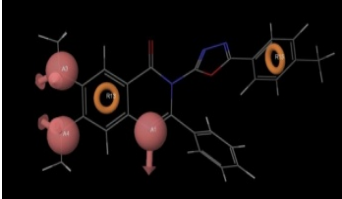

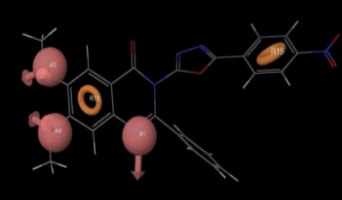
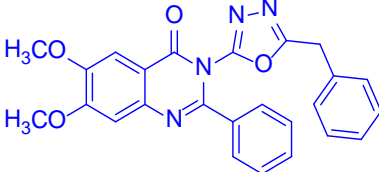
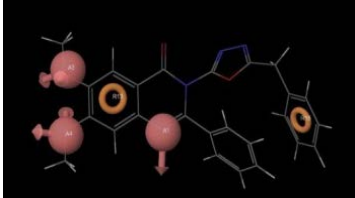
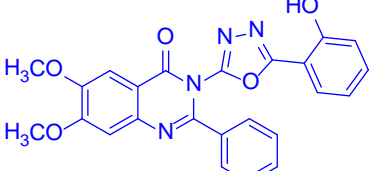
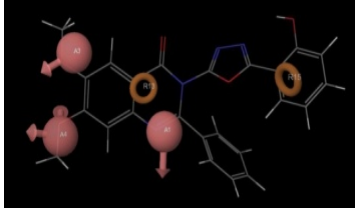
Code	Compounds	Pharmacophoric Fitness	Predicted Activity (IC <sub>50</sub> )
25			3.402
26			1.703
27			3.227
28			2.305
29			1.365
30			4.241

Table 4 Continue

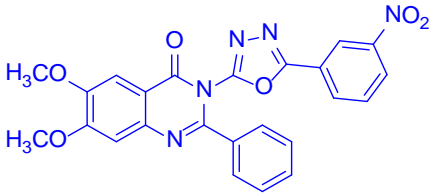
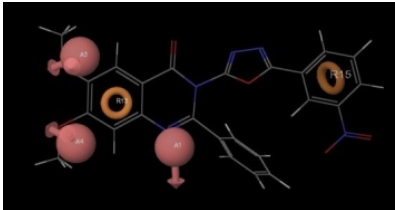
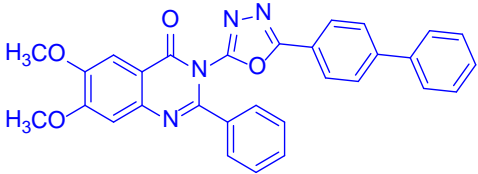
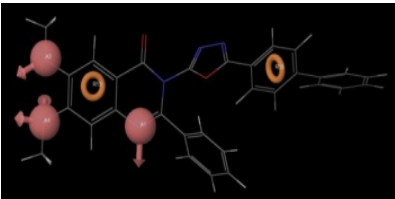
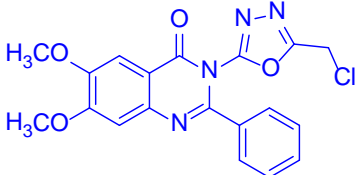
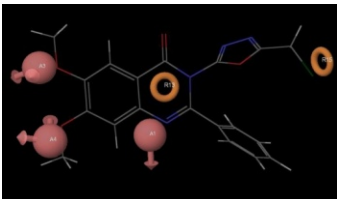
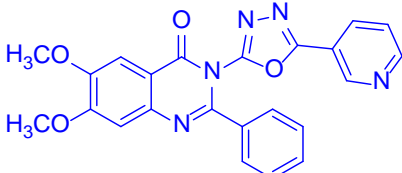
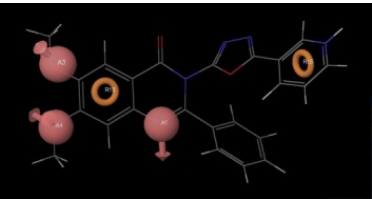
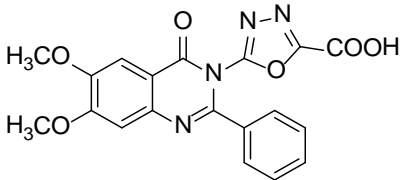
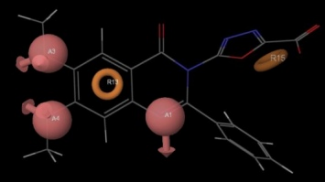
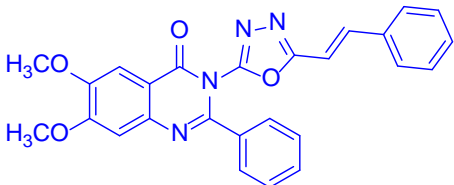
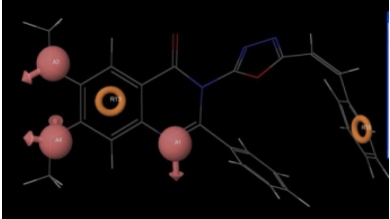
Code	Compounds	Pharmacophoric Fitness	Predicted Activity (IC <sub>50</sub> )
31			3.280
32			2.285
33			3.252
34			0.993
35			4.076
36			2.192



Table 4 Continue

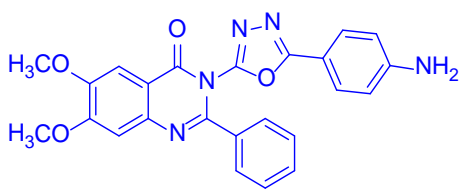
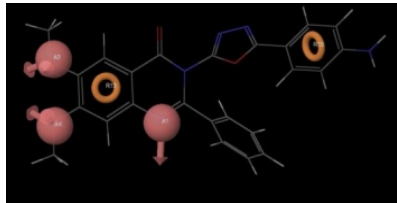
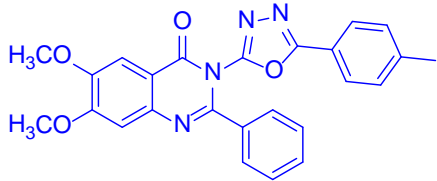
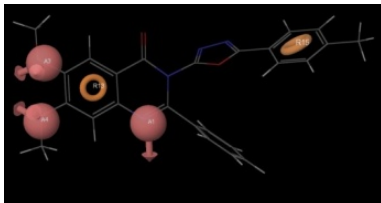
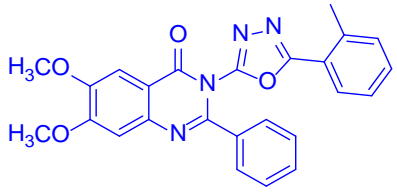
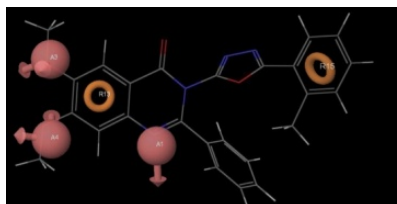
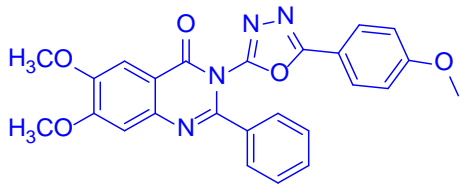
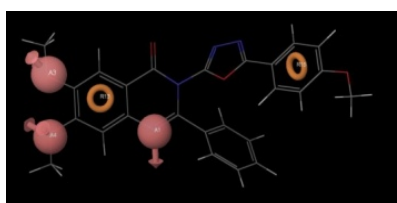
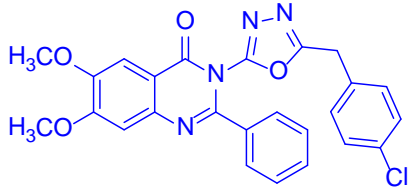
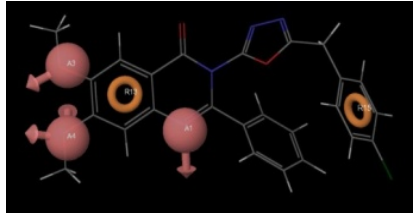
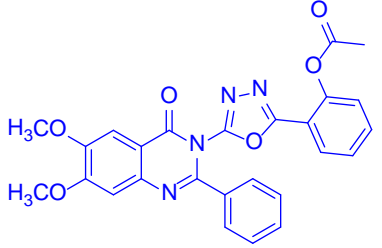
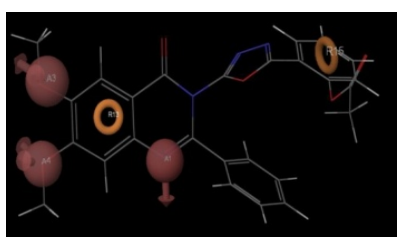
Code	Compounds	Pharmacophoric Fitness	Predicted Activity (IC <sub>50</sub> )
37			4.285
38			3.296
39			3.329
40			0.526
41			0.851
42			2.193

Table 4 Continue

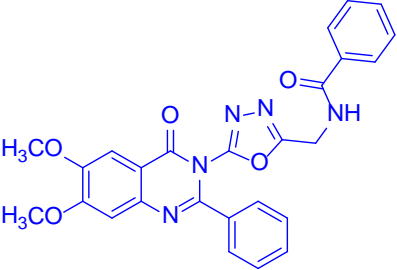
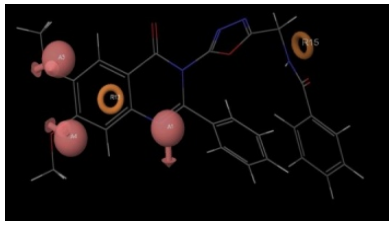
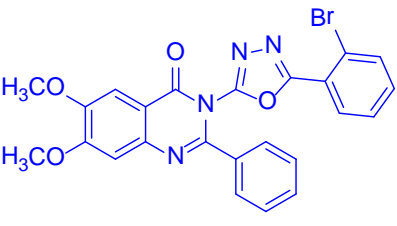
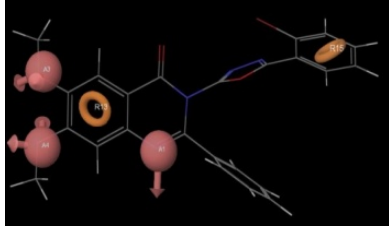
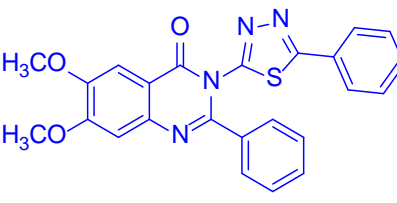
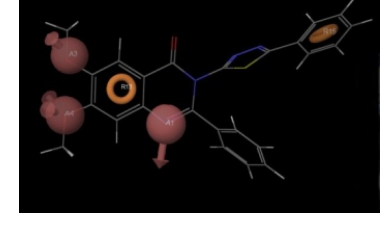
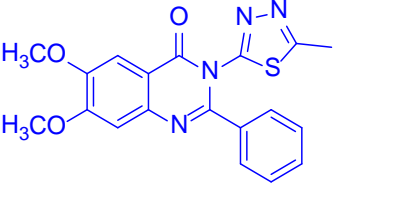
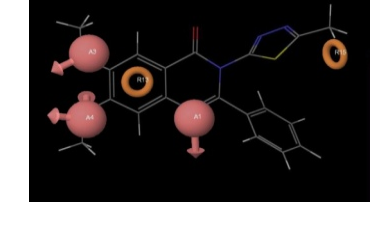
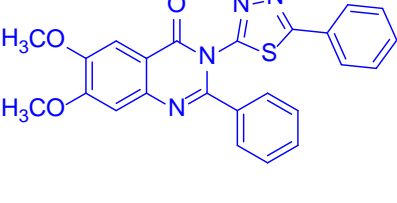
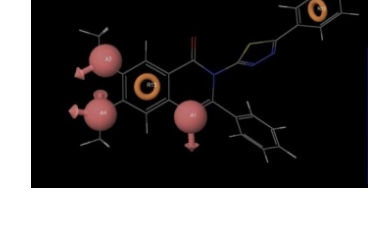
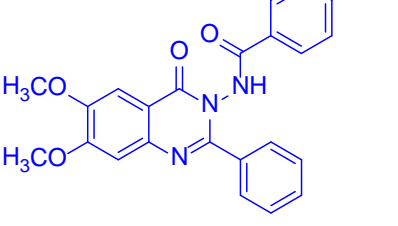
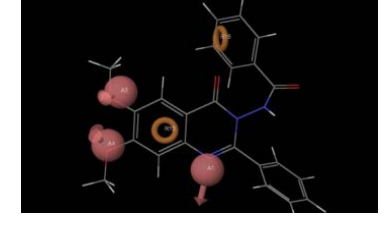
Code	Compounds	Pharmacophoric Fitness	Predicted Activity (IC <sub>50</sub> )
43			4.350
44			3.181
45			1.528
46			1.642
47			0.184
48			4.203

Table 4 Continue

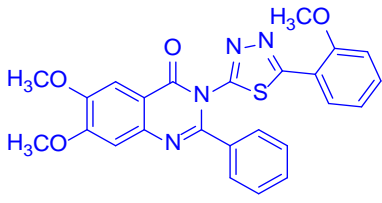
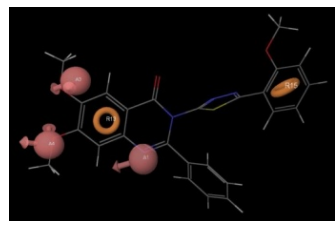
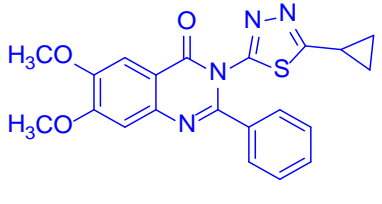
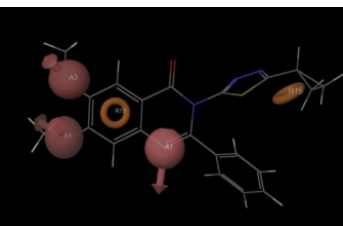
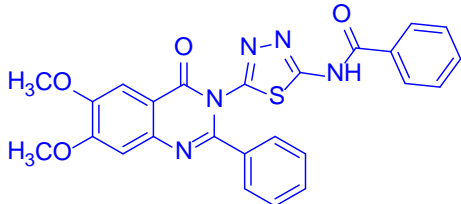
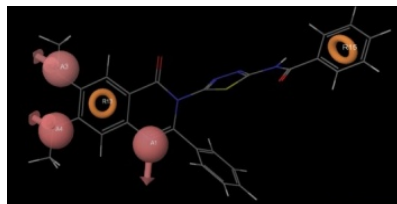
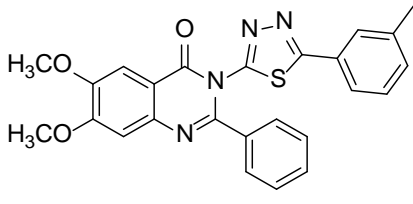
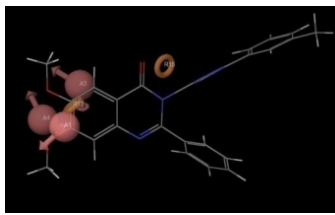
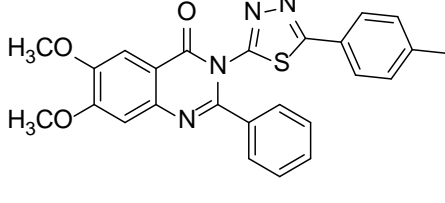
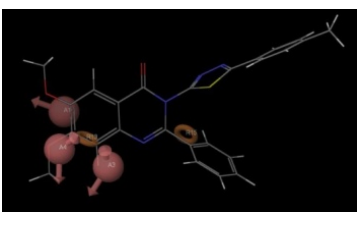
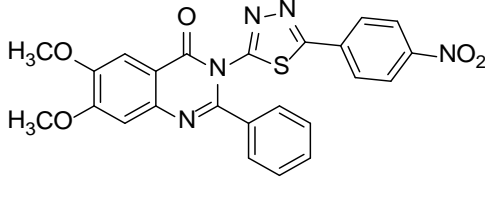
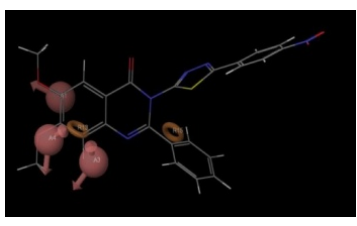
Code	Compounds	Pharmacophoric Fitness	Predicted Activity (IC <sub>50</sub> )
49			4.299
50			0.952
51			1.275
52			11.013
53			9.076
54			10.076

Table 4 Continue

Code	Compounds	Pharmacophoric Fitness	Predicted Activity (IC <sub>50</sub> )
55			1.358
56			8.083
57			3.346
58			12.002
59			4.136
60			9.009

Table 4 Continue

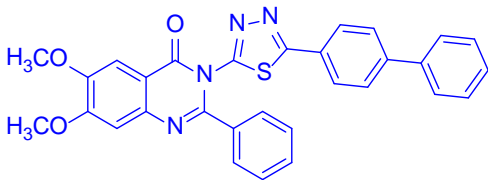
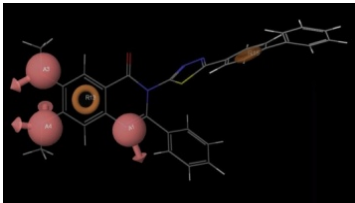
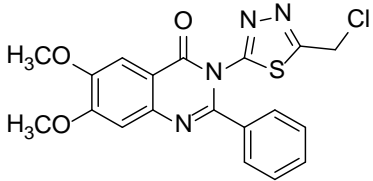
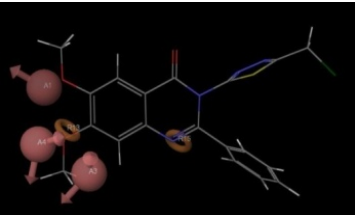
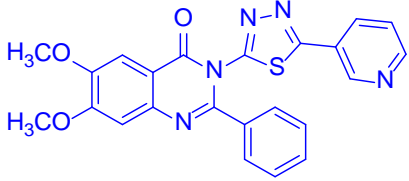
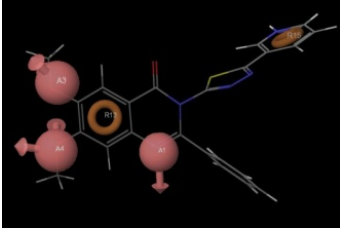
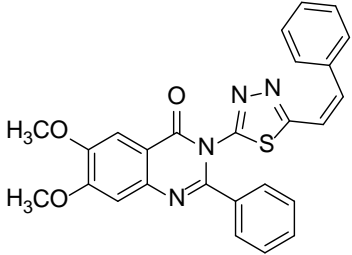
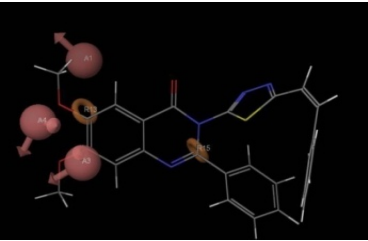
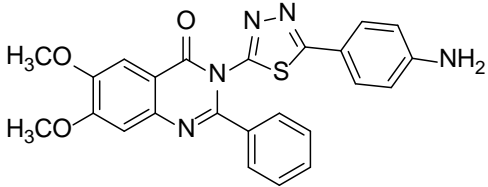
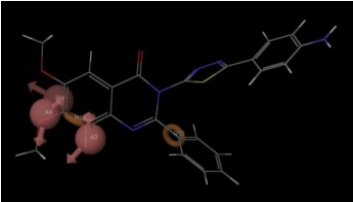
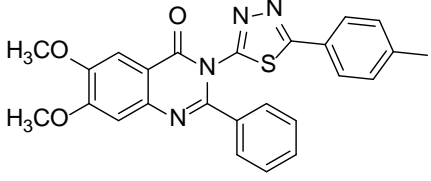
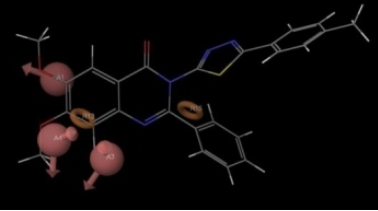
Code	Compounds	Pharmacophoric Fitness	Predicted Activity (IC <sub>50</sub> )
61			5.176
62			11.053
63			0.966
64			8.064
65			7.166
66			6.076

Table 4 Continue

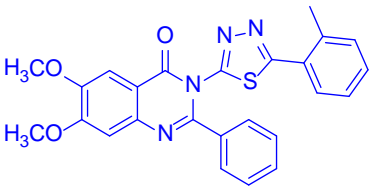
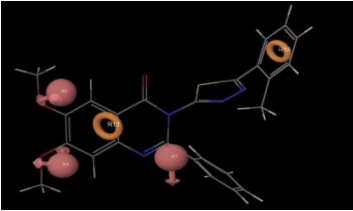
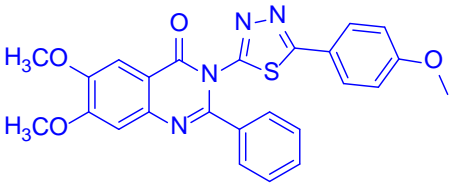
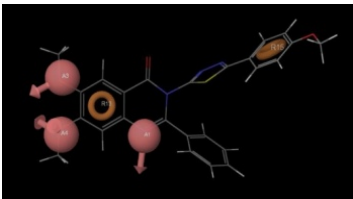
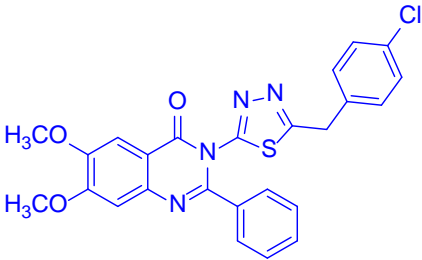
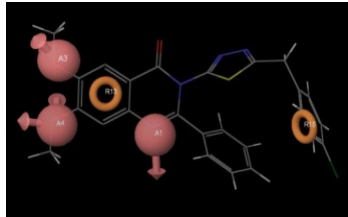
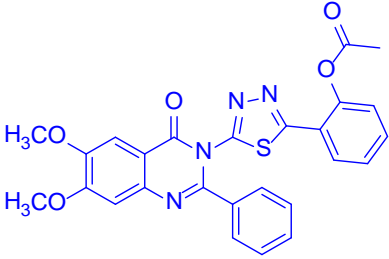
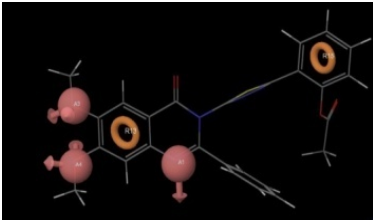
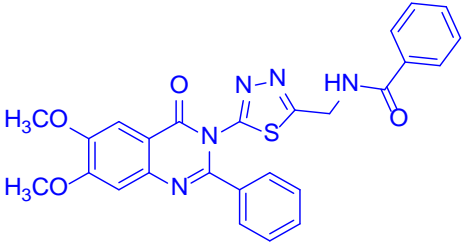
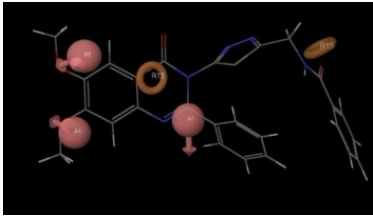
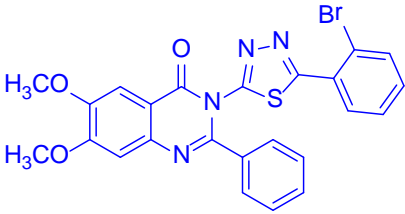
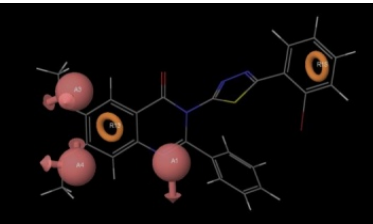
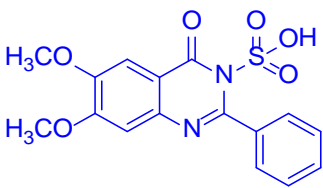
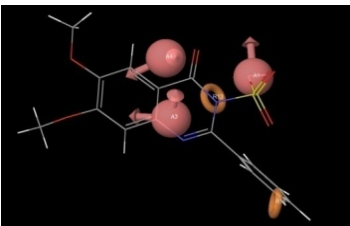
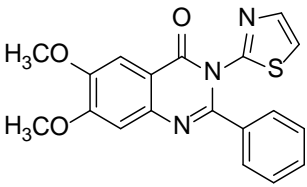
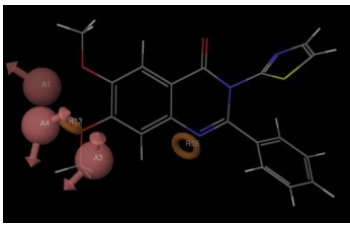
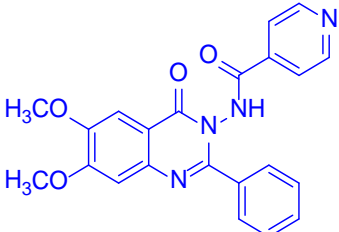
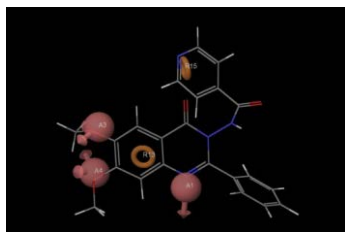
Code	Compounds	Pharmacophoric Fitness	Predicted Activity (IC <sub>50</sub> )
67			4.157
68			0.191
69			0.213
70			3.286
71			2.215
72			4.191

Table 4 Continue

Code	Compounds	Pharmacophoric Fitness	Predicted Activity (IC <sub>50</sub> )
73			5.158
74			13.095
75			4.212

\* Blue colour compounds with good alignment score and predicted activity is selected for the next filter (Docking Study).

**Table 5** Glide docking results of quinazoline derivatives based on glide dock score, glide energy and hydrogen bonding interaction.

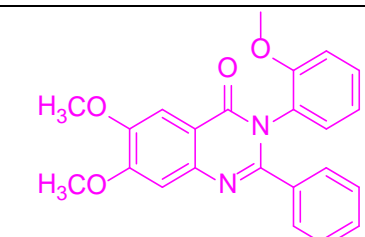

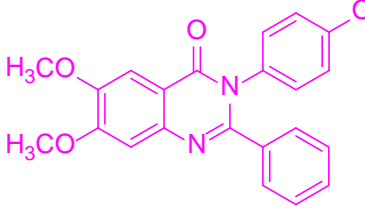
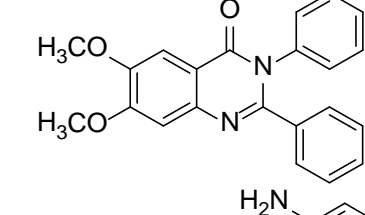
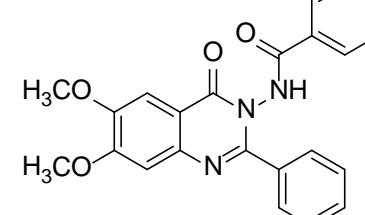
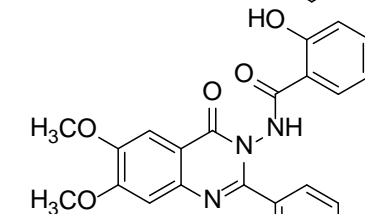
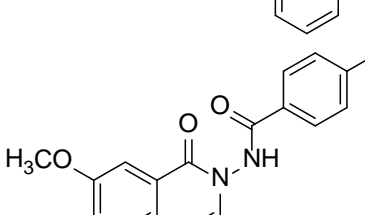
Code	Compounds	Docking Score	Glide Energy (kcal/mol)	H-bond interaction
2		-7.583	-61.7243	N- of quinazoline and H atom of amino acid backbone of CYS-919
3		-7.956	-75.4361	N- of quinazoline and H atom of amino acid backbone of CYS-919
10		-8.687	-81.3081	N- of quinazoline and H atom of amino acid backbone of CYS-919
14		-4.2775	-32.5766	N- of quinazoline and H atom of amino acid backbone of CYS-919
16		-3.6592	-28.1827	N- of quinazoline and H atom of amino acid backbone of CYS-919
18		-4.6680	-37.9244	N- of quinazoline and H atom of amino acid backbone of CYS-919
19		-4.0451	-38.7657	N- of quinazoline and H atom of amino acid backbone of CYS-919



Table 5 Continue

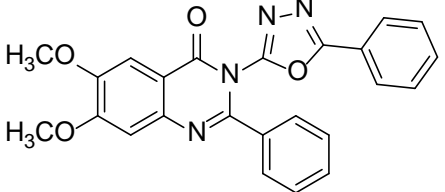
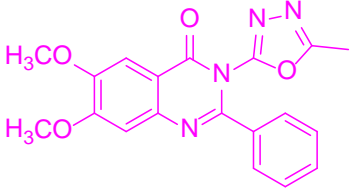
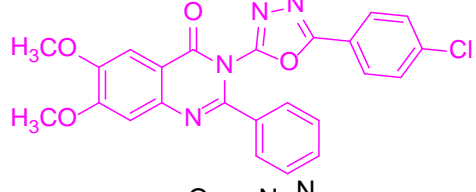
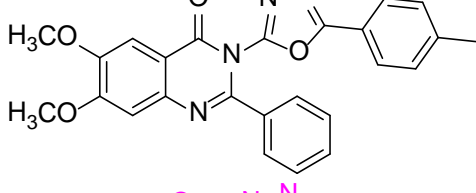
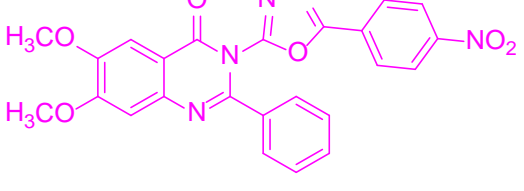
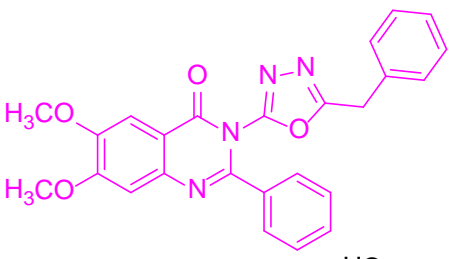
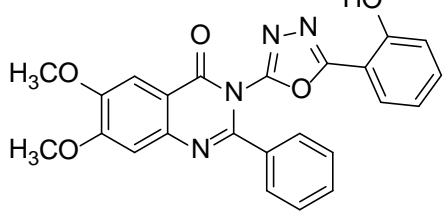

Code	Compounds	Docking Score	Glide Energy (kcal/mol)	H-bond interaction
20		-3.9235	-29.5729	N- of quinazoline and H atom of amino acid backbone of CYS-919
21		-7.6289	-63.2202	N- of quinazoline and H atom of amino acid backbone of CYS-919
22		-9.11	-86.8795	N- of quinazoline and H atom of amino acid backbone of CYS-919
27		-4.1484	-38.6999	N- of quinazoline and H atom of amino acid backbone of CYS-919
28		-5.8039	-52.3077	N- of quinazoline and H atom of amino acid backbone of CYS-919
29		-7.80	-70.0314	N- of quinazoline and H atom of amino acid backbone of CYS-919
30		-5.7739	-43.0027	N- of quinazoline and H atom of amino acid backbone of CYS-919
31		-6.7289	-51.1708	N- of quinazoline and H atom of amino acid backbone of CYS-919

Table 5 Continue

Code	Compounds	Docking Score	Glide Energy (kcal/mol)	H-bond interaction
32		-6.5020	-53.2851	N- of quinazoline and H atom of amino acid backbone of CYS-919
33		-5.1942	-40.6320	N- of quinazoline and H atom of amino acid backbone of CYS-919
34		-8.1133	-77.5216	N- of quinazoline and H atom of amino acid backbone of CYS-919
36		-5.7164	-43.6706	N- of quinazoline and H atom of amino acid backbone of CYS-919
41		-8.5383	-80.3714	N- of quinazoline and H atom of amino acid backbone of CYS-919
42		-4.6402	-38.8968	N- of quinazoline and H atom of amino acid backbone of CYS-919
43		-5.2584	-50.8655	N- of quinazoline and H atom of amino acid backbone of CYS-919

Table 5 Continue

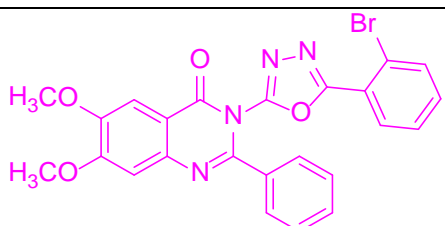
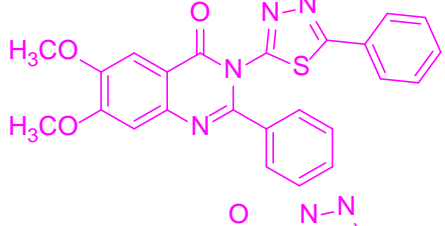
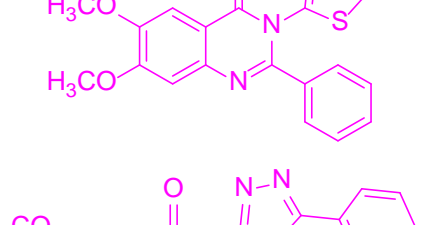
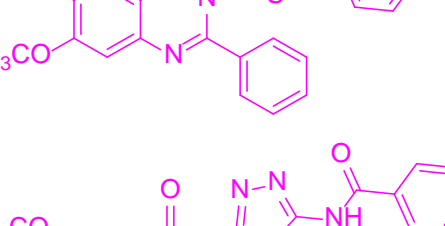
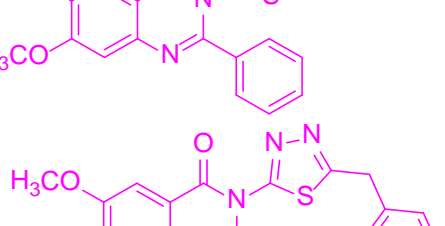
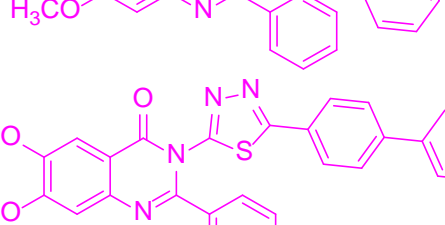
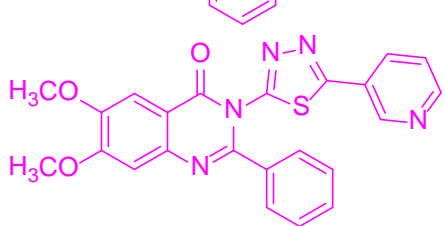

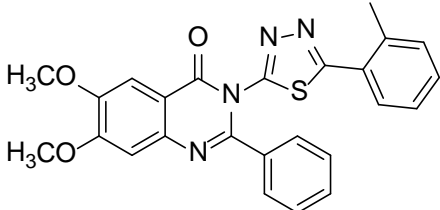



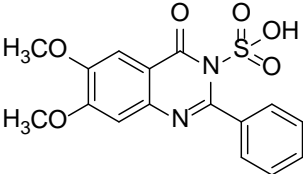
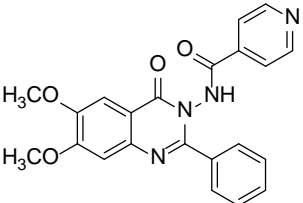
Code	Compounds	Docking Score	Glide Energy (kcal/mol)	H-bond interaction
44		-7.7567	-61.2602	N- of quinazoline and H atom of amino acid backbone of CYS-919
45		-7.7435	-68.6023	N- of quinazoline and H atom of amino acid backbone of CYS-919
46		-7.7005	-66.5236	N- of quinazoline and H atom of amino acid backbone of CYS-919
47		-10.89	-90.9803	N- of quinazoline and H atom of amino acid backbone of CYS-919
51		-7.90	-74.3078	N- of quinazoline and H atom of amino acid backbone of CYS-919
55		-7.5070	-72.4362	N- of quinazoline and H atom of amino acid backbone of CYS-919
61		-6.3233	-53.3556	N- of quinazoline and H atom of amino acid backbone of CYS-919
63		-8.21	-78.2110	N- of quinazoline and H atom of amino acid backbone of CYS-919

Table 5 Continue

Code	Compounds	Docking Score	Glide Energy (kcal/mol)	H-bond interaction
67		-4.1677	-42.3851	N- of quinazoline and H atom of amino acid backbone of CYS-919
68		-10.62	-88.9761	N- of quinazoline and H atom of amino acid backbone of CYS-919
69		-9.25	-87.8231	N- of quinazoline and H atom of amino acid backbone of CYS-919
72		-6.1185	-54.2228	N- of quinazoline and H atom of amino acid backbone of CYS-919
73		-3.5910	-25.9877	N- of quinazoline and H atom of amino acid backbone of CYS-919
75		-3.2501	-24.4840	N- of quinazoline and H atom of amino acid backbone of CYS-919

\* Pink colour compounds with good docking score and glide energy is selected for the next filter (Lipinski's Rule).

Table 6 Lipinski's rule of five for drug likeliness by QikProp.

Criteria	Lipinski's Rule of Five (Drug Likeliness)					
Sr. No.	Compounds	Molecular Weight	H-bond donor	H-bond acceptor	QPlogP O/W <sup>a</sup>	Violation of Lipinski's Rule
2		388.422	00	6.250	4.117	00
3		392.841	00	5.500	4.633	00
10		388.422	00	6.250	4.186	00
21		364.360	00	8.000	2.133	00
22		460.876	00	8.000	4.042	00
23		456.457	00	8.750	3.748	00
24		390.398	00	8.000	2.995	00
26		440.457	00	8.000	3.794	00

Table 6 Continue

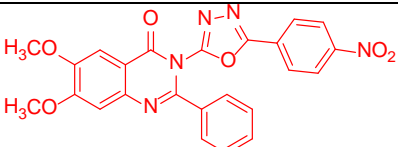
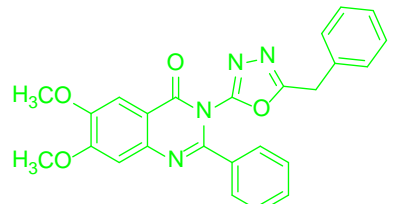
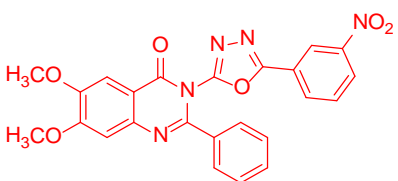
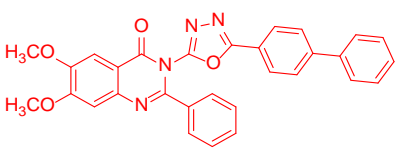
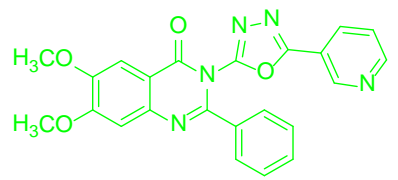
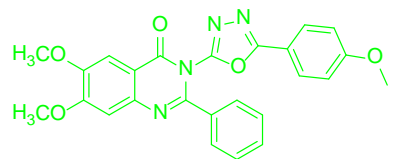
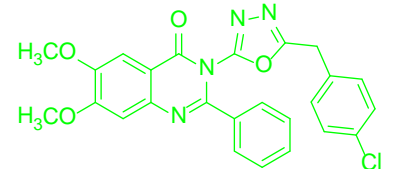
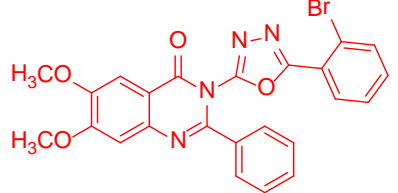
Sr.No.	Compounds	Lipinski's Rule of Five (Drug Likeliness)				
		Molecular Weight	H-bond donor	H-bond acceptor	QPlogP O/W <sup>a</sup>	Violation of Lipinski's Rule
28		471.428	00	9.000	2.780	01
29		440.457	00	8.000	3.967	00
31		471.428	00	9.000	2.780	01
32		502.528	00	8.000	5.210	02
34		427.418	00	9.500	2.480	00
40		456.457	00	8.750	3.594	00
41		474.902	00	8.000	4.495	00
44		505.327	00	8.000	3.871	01

Table 6 Continue

Sr.No.	Compounds	Lipinski's Rule of Five (Drug Likeliness)				
		Molecular Weight	H-bond donor	H-bond acceptor	QPlogP O/W <sup>a</sup>	Violation of Lipinski's Rule
45		442.491	00	7.500	4.244	00
46		380.420	00	7.500	2.836	00
47		476.936	00	7.500	4.725	00
50		406.458	00	7.500	3.354	00
51		485.516	1.000	10.000	3.720	00
55		456.518	00	7.500	4.607	00
61		518.589	00	7.500	5.893	02
63		443.479	00	9.000	3.168	00

Table 6 Continue

Criteria	Lipinski's Rule of Five (Drug Likeliness)						
	Sr.No.	Compounds	Molecular Weight	H-bond donor	H-bond acceptor	QPlogP O/W <sup>a</sup>	Violation of Lipinski's Rule
	68		472.517	00	8.250	4.278	00
	69		490.963	00	7.500	4.986	00
	70		500.528	00	10.000	3.521	01
	72		521.387	00	7.500	4.415	01

\* Green colour compounds with no violation of Lipinski's Rule is selected for the synthesis



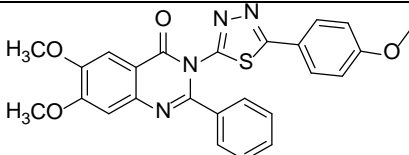
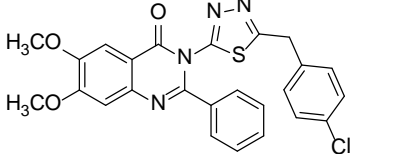
**Table 7** Inhibitory profile of virtually screened synthesized derivatives against VEGFR-2 kinase and HUVEC proliferation ( $IC_{50}$ /nm)

Compound	Structure	VEGFR-2 <sup>a</sup>	HUVEC (VEGF) <sup>b</sup>
2		124	15
3		50	233
10		16	179
21		112	46
22		12	18
23		15	67
24		45	196
26		107	78
29		87	258

Table 7 Continue

Compound	Structure	VEGFR-2 <sup>a</sup>	HUVEC (VEGF) <sup>b</sup>
34		45	196
40		13.5	13.6
45		98	324
46		102	77
47		3.8	5.5
50		25	89
51		65	237
55		73	308
63		35	187

Table 7 Continue

Compound	Structure	VEGFR-2 <sup>a</sup>	HUVEC (VEGF) <sup>b</sup>
68		5.5	12.9
69		9.6	19.8

<sup>a</sup> IC<sub>50</sub> values were averaged values determined by at least two independent experiments.

<sup>b</sup> Human umbilical vein endothelial cells.

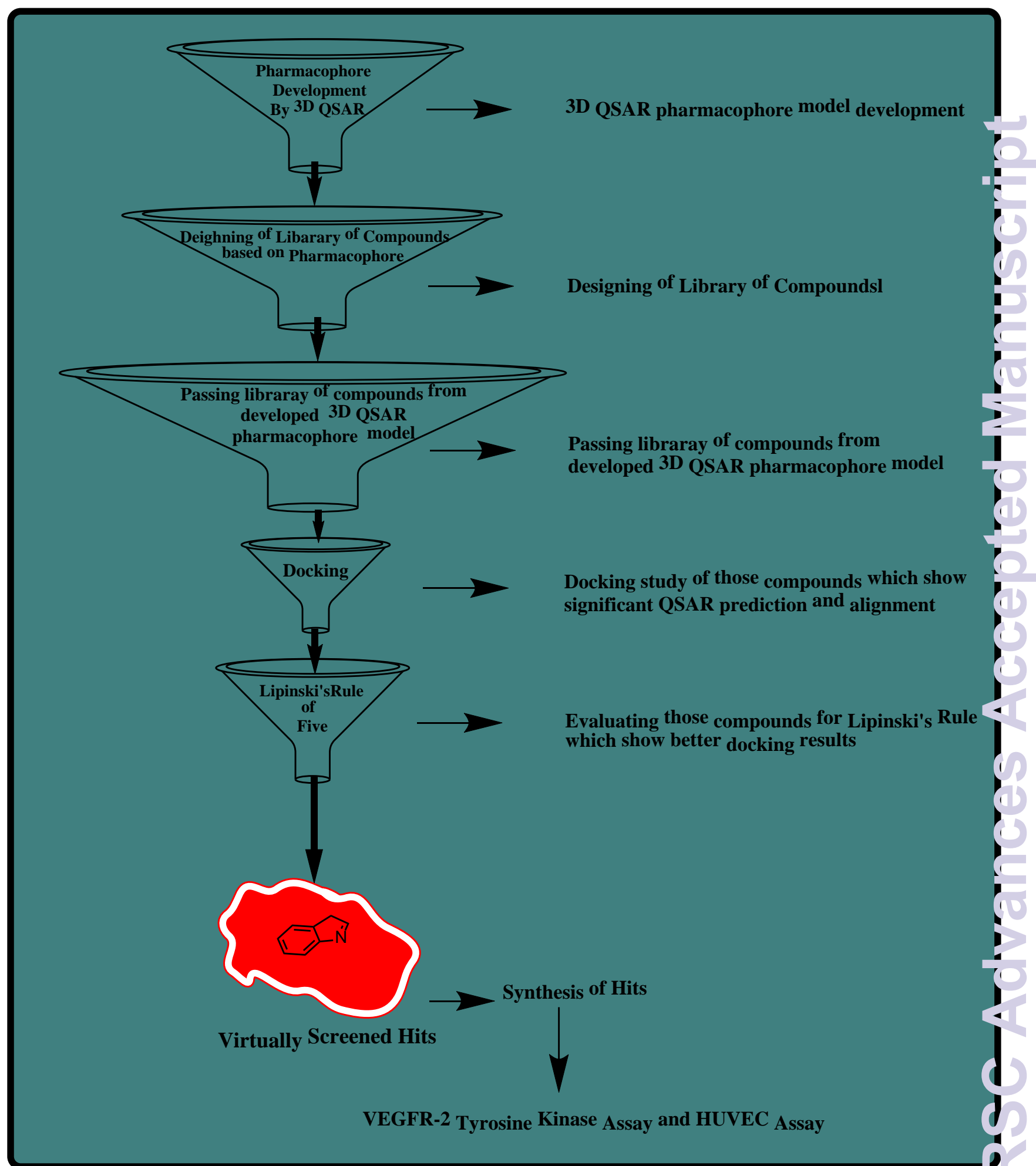
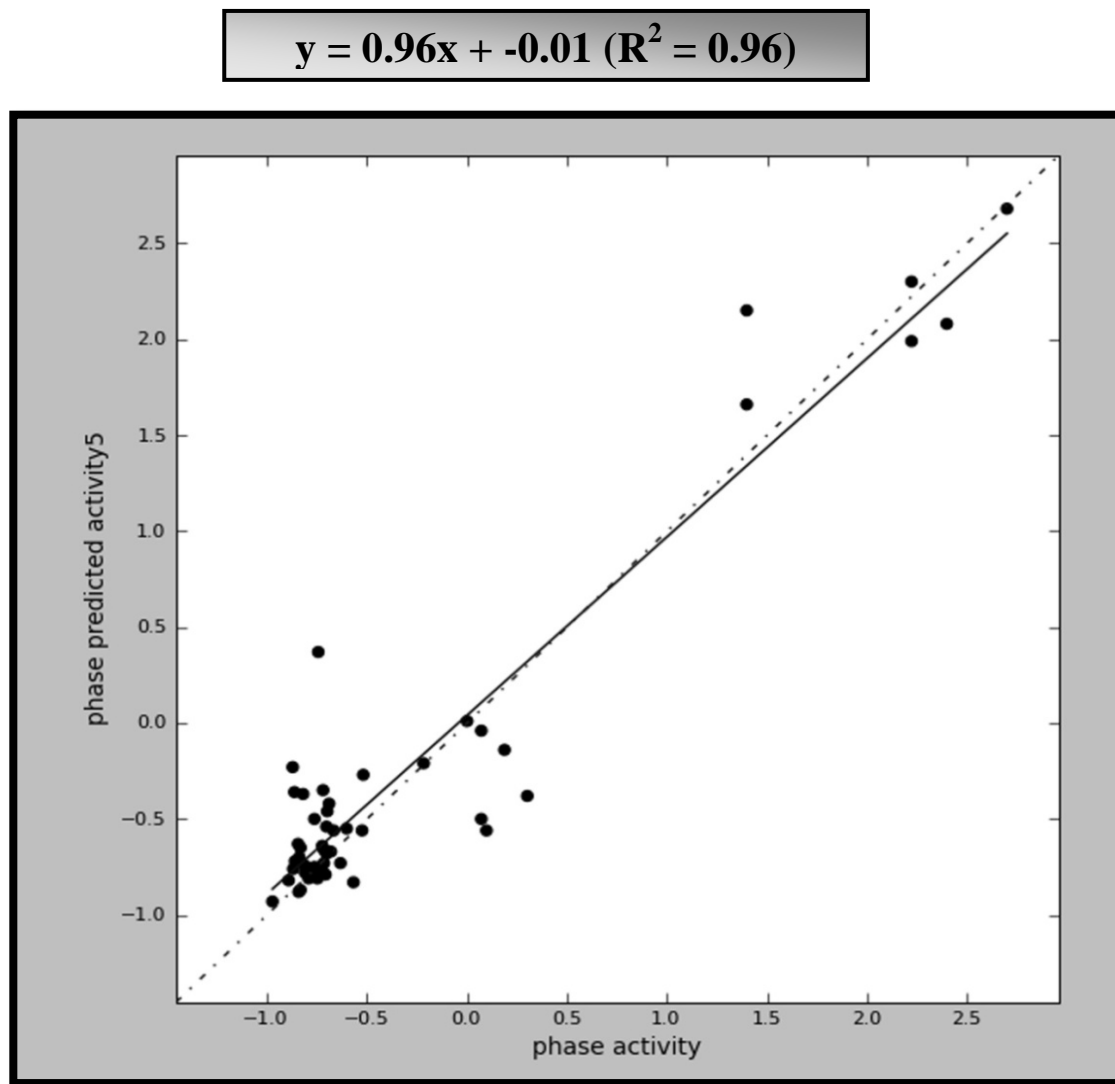
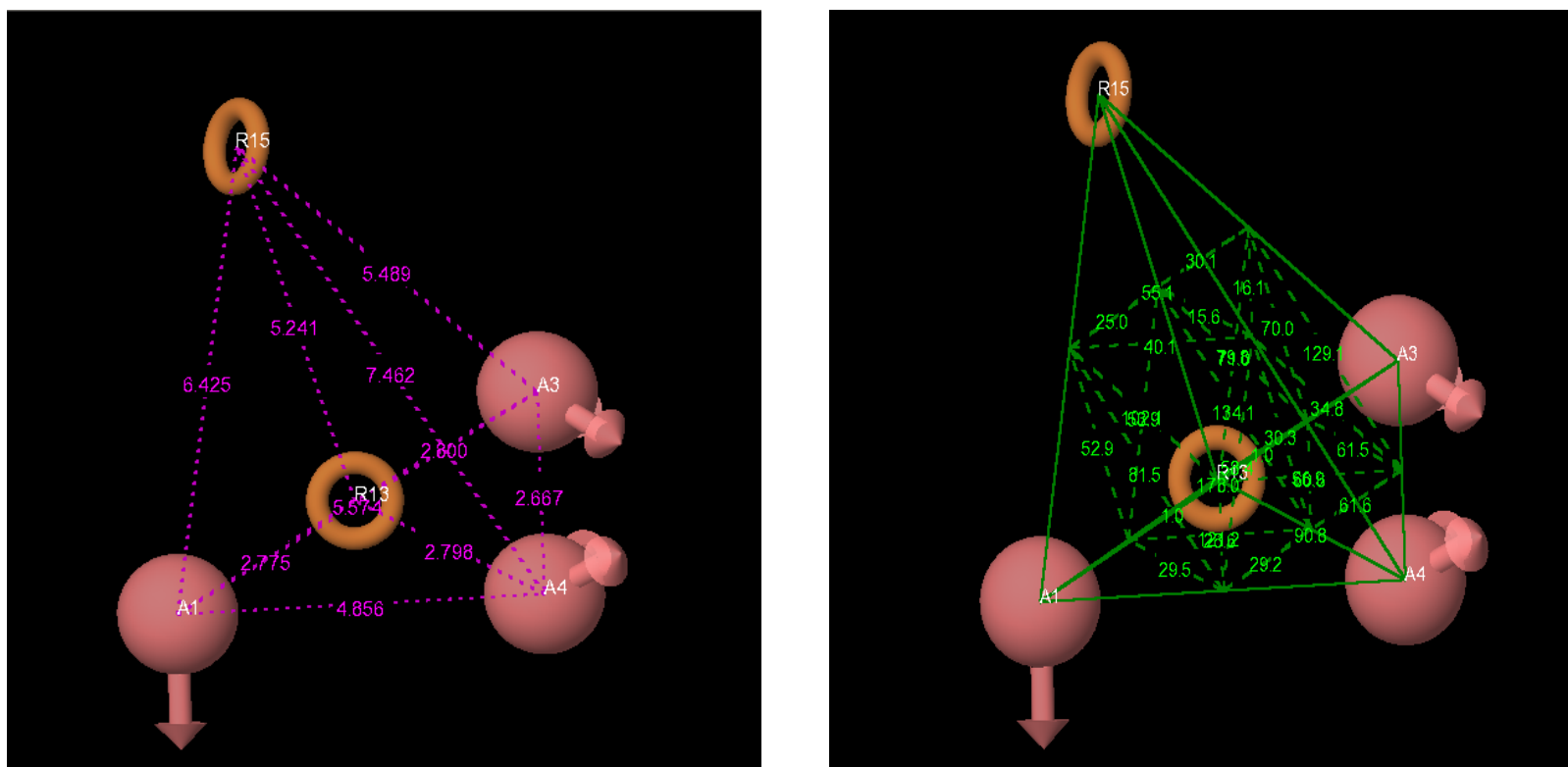


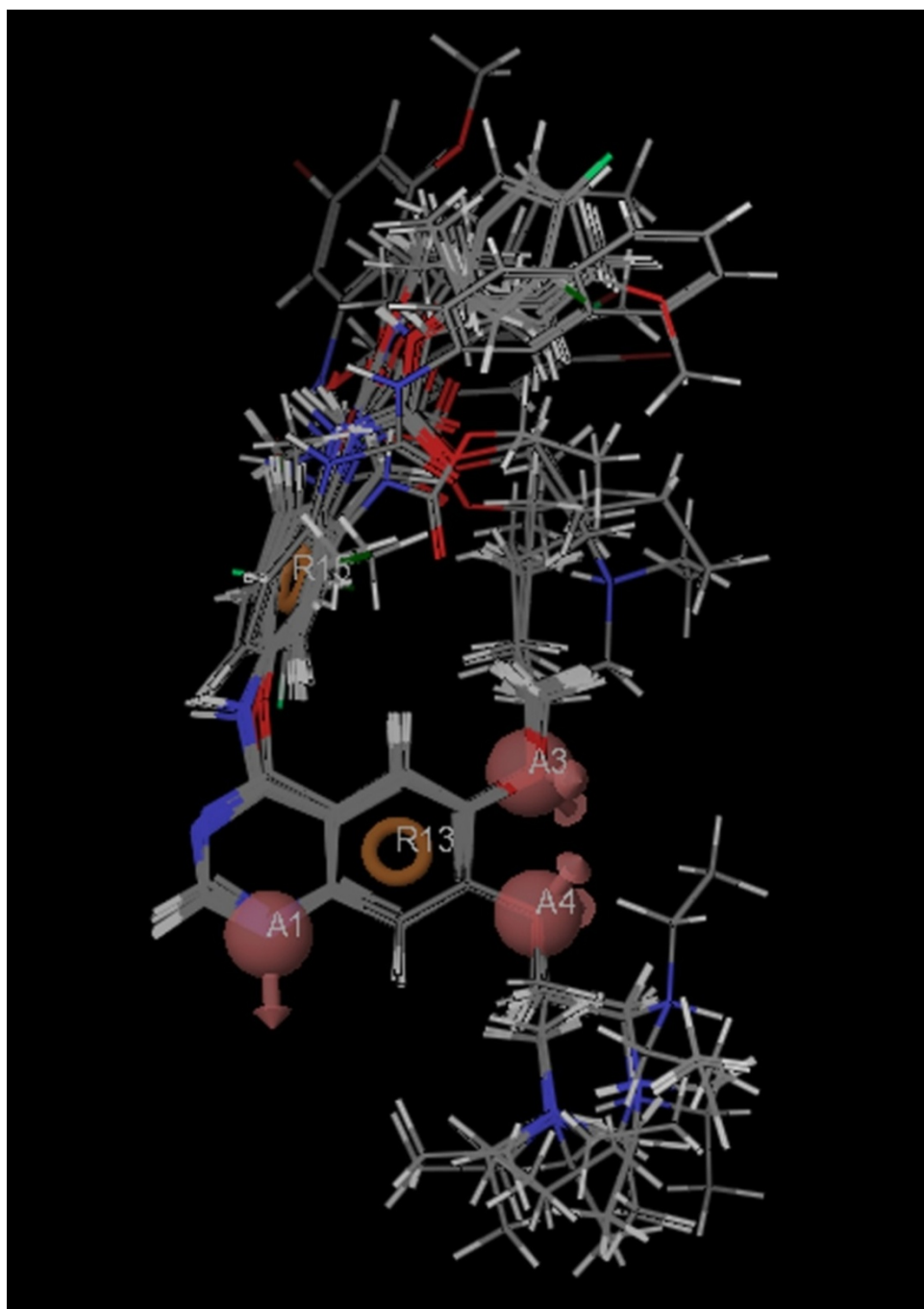
Fig. 1 Virtual screening flow chart



**Fig. 2** Scatter plots for the QSAR model applied to all compounds in the training and test set.



**Fig. 3** Pharmacophore hypothesis (AAARR.8), where red ball shows hydrogen bond acceptor site, while the brown ring demonstrates the R (ring) feature pharmacophore distances (A) and angles (B) between pharmacophoric sites.



**Fig. 4** The common pharmacophore based alignment of molecules in 3D QSAR

RSC Advances Accepted Manuscript





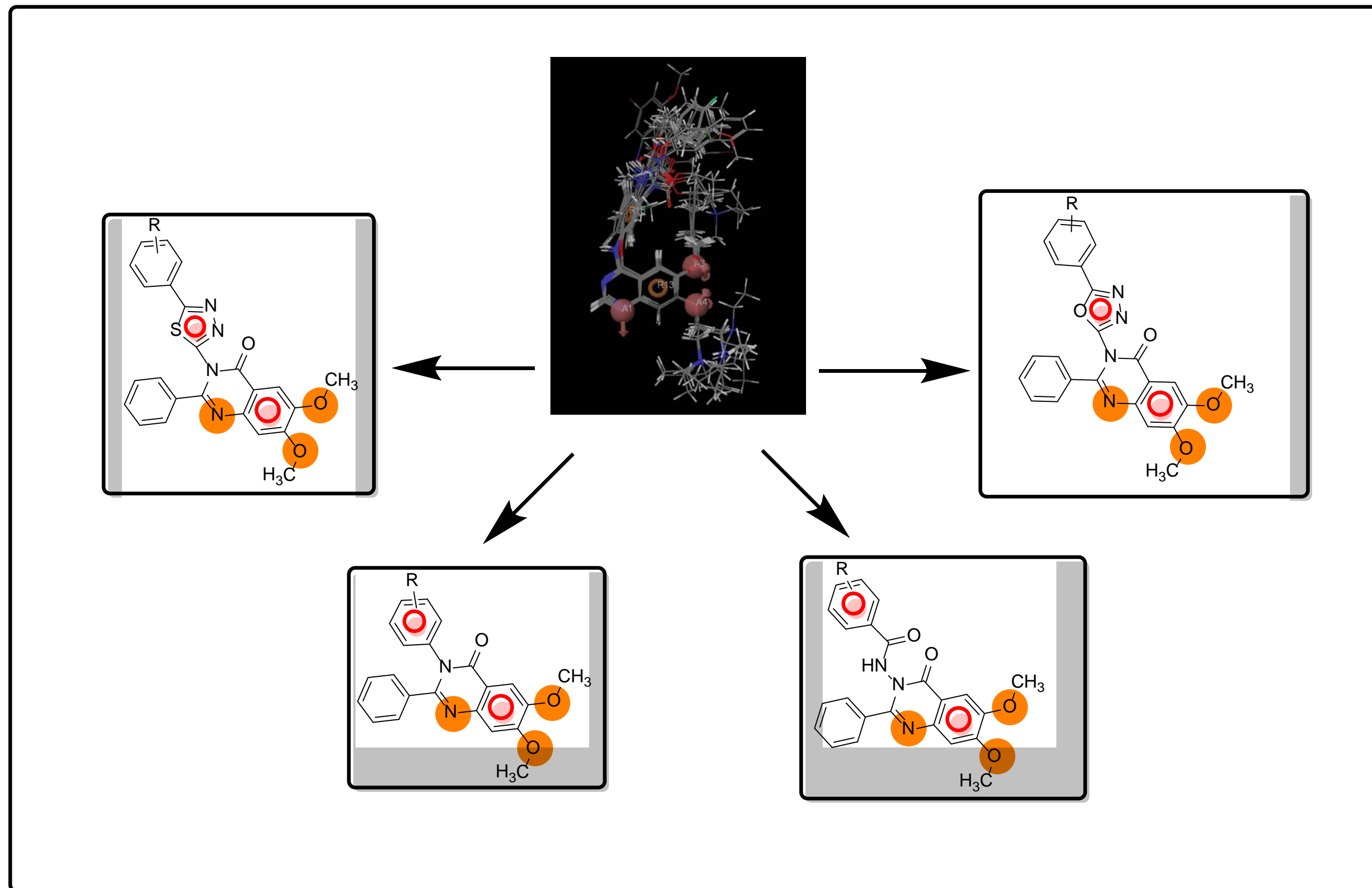


Fig. 5 Designing of the library of compounds based upon the developed 3D QSAR pharmacophore model



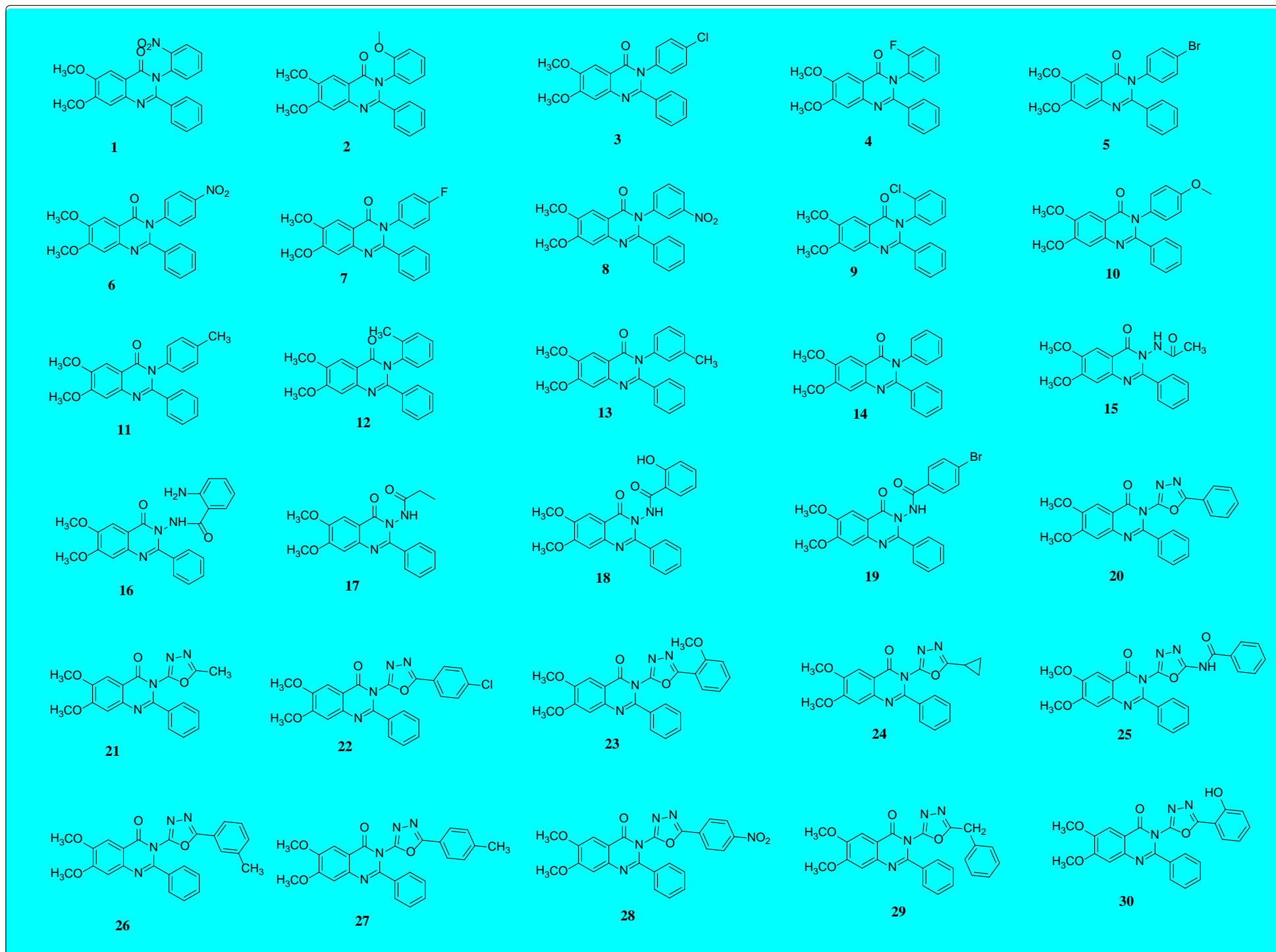
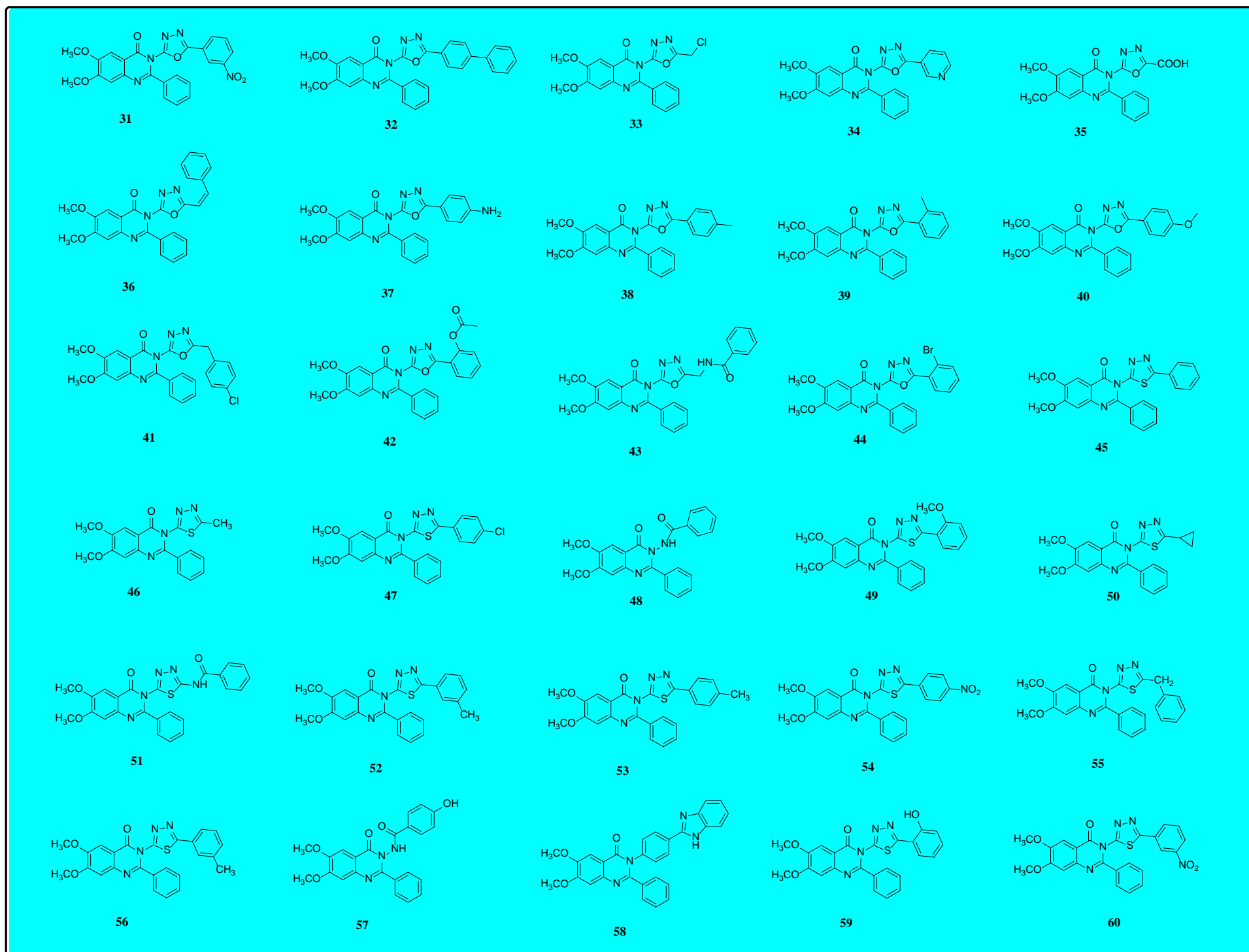


Fig. 6 (A) Designed library based upon 3D QSAR model



**Fig. 6 (B)** Designed library based upon 3D QSAR model

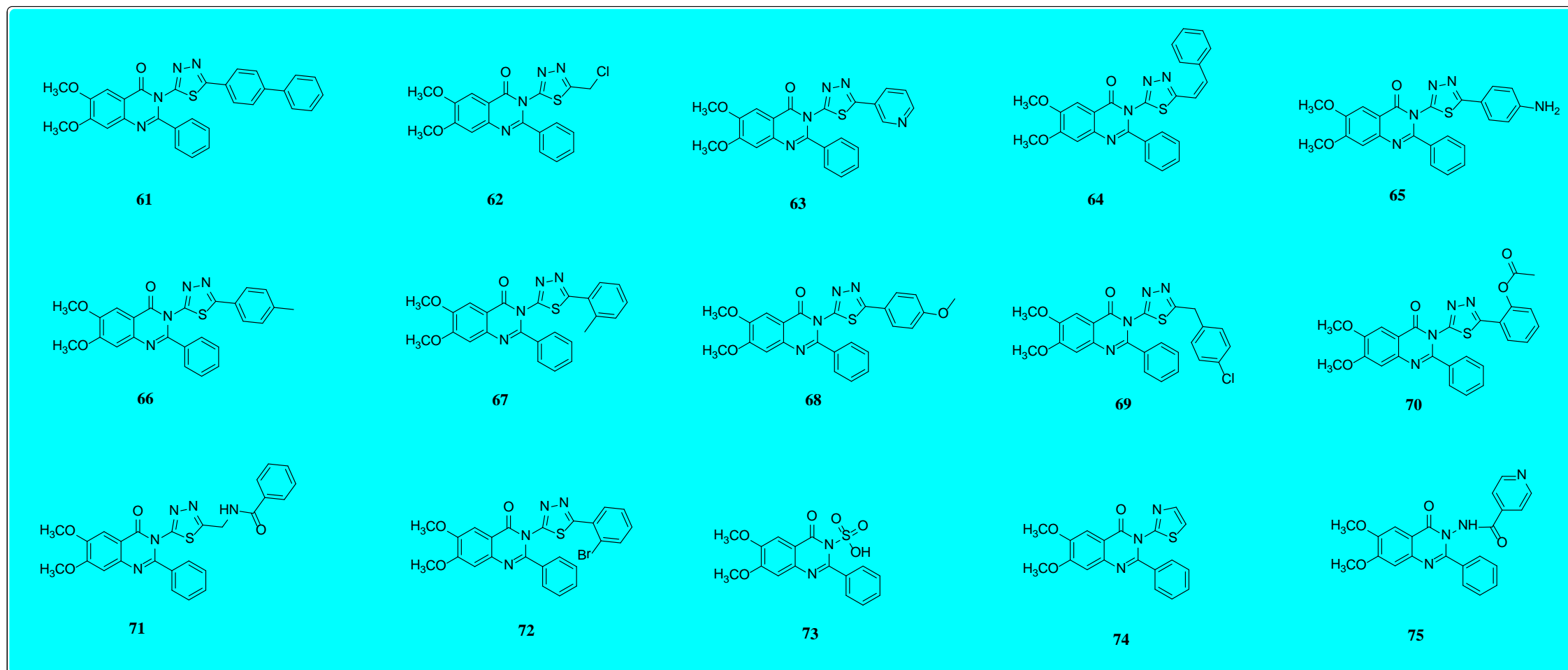
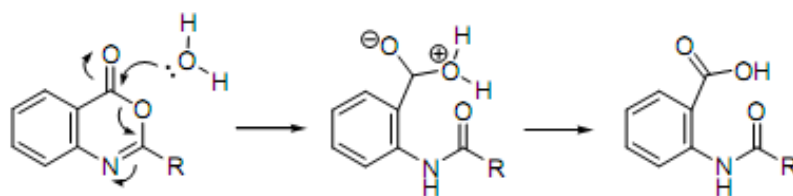
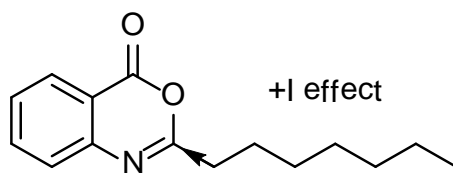


Fig. 6 (C) Designed library based upon 3D QSAR model





**Fig. 7** Ring opening of benzoxazinone by water



**Fig. 8** Impact of electron donating group at C-2 over the reactivity of benzoxazinone



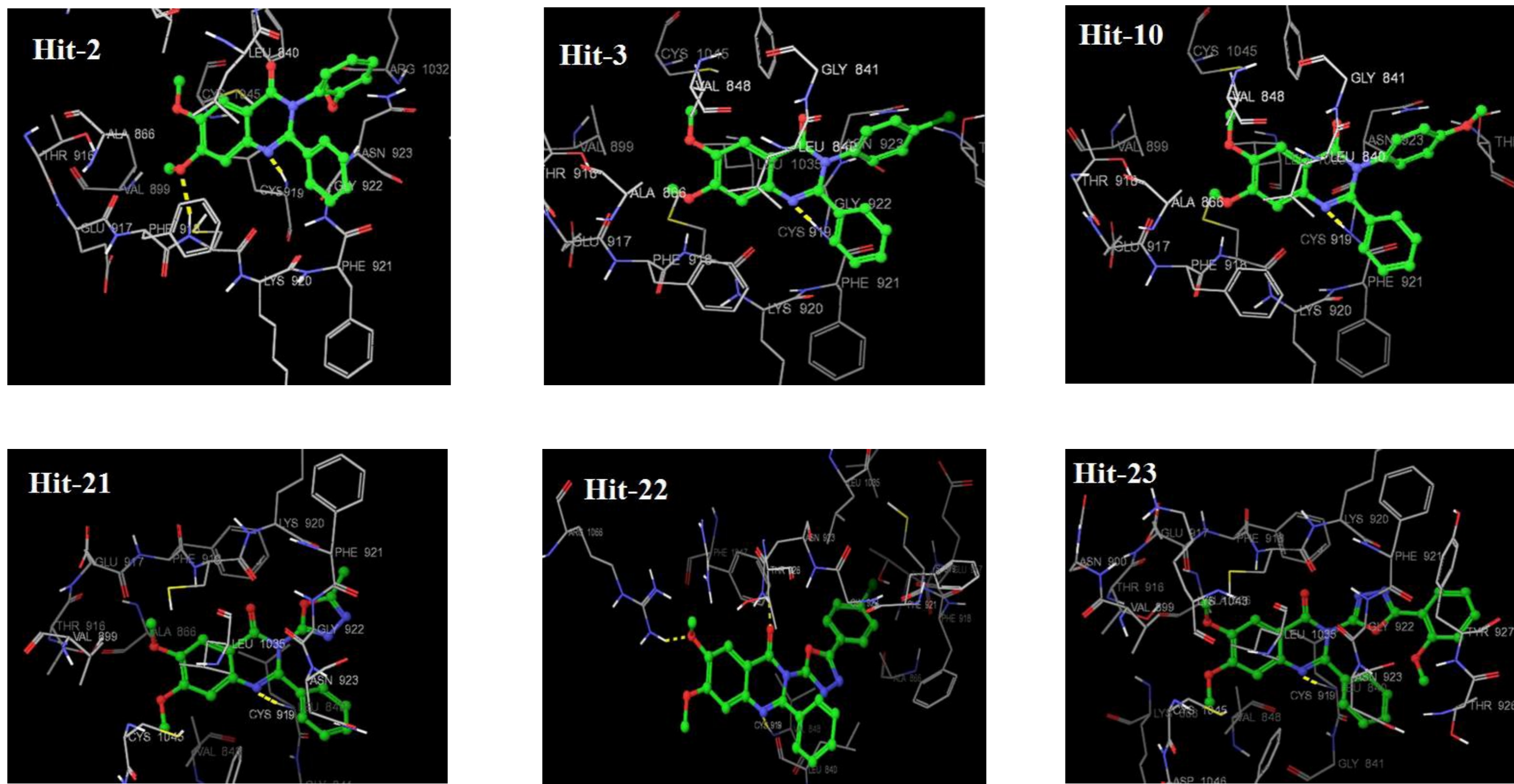
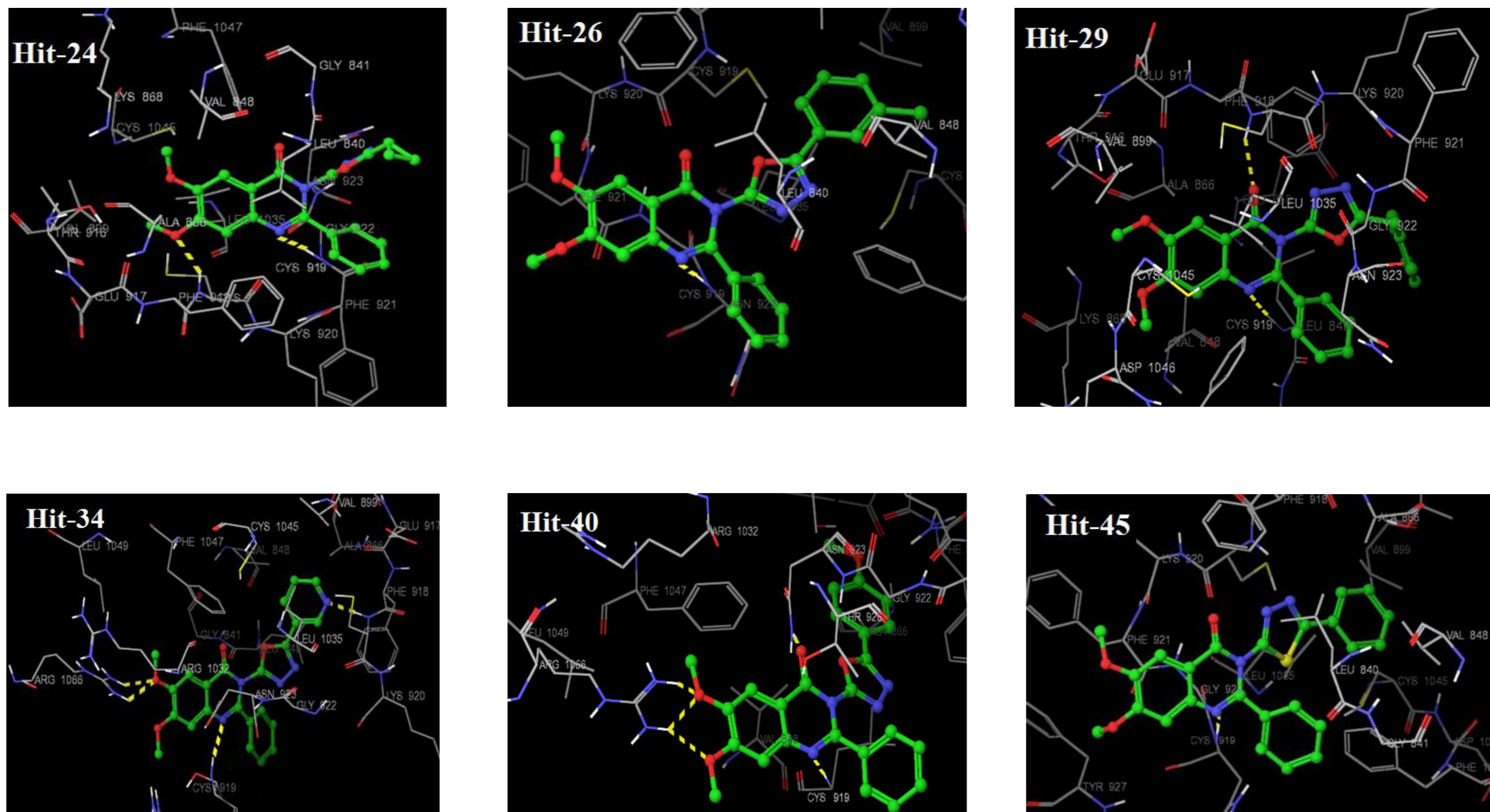


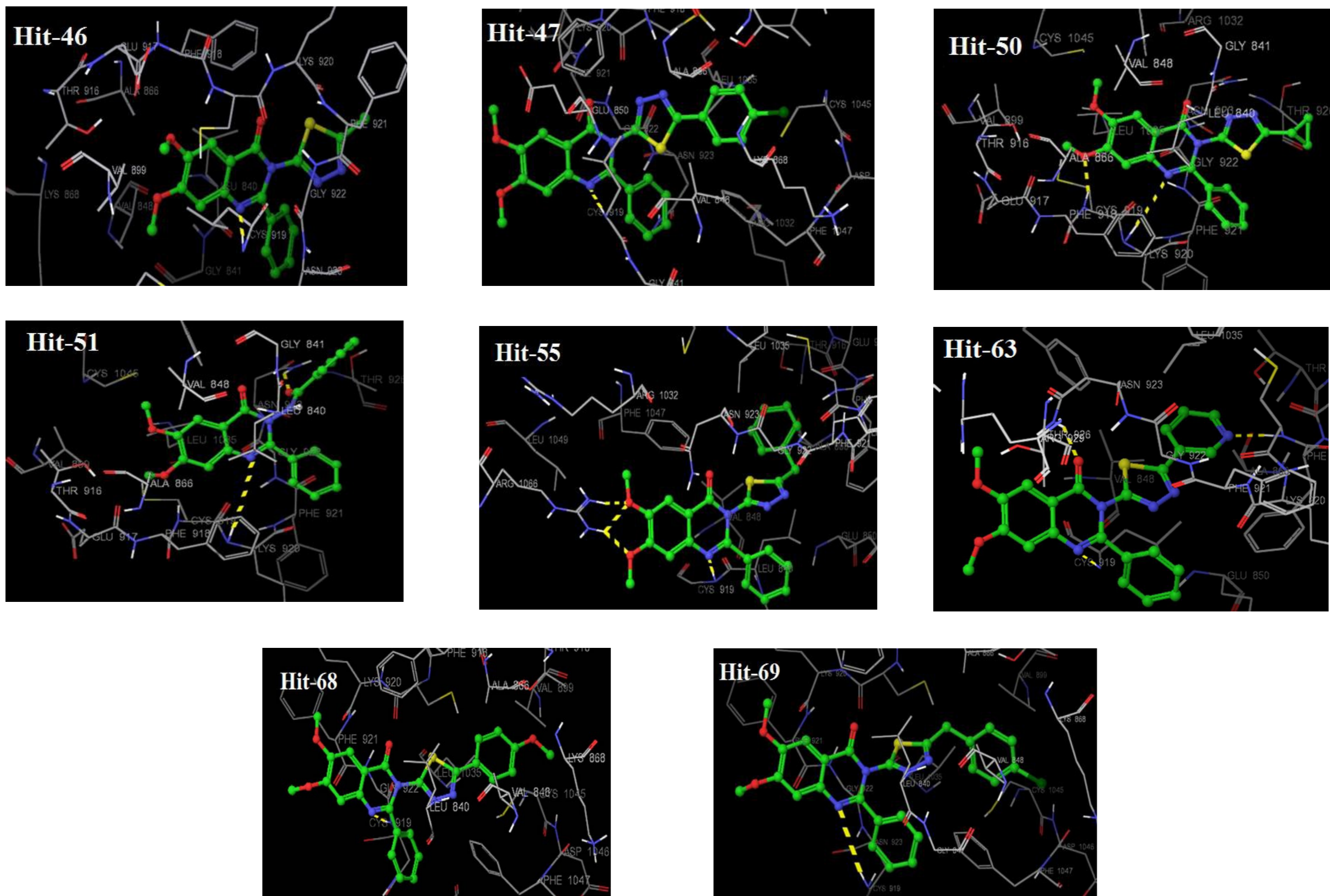
Fig. 9 Binding interaction of Hits with VEGFR-2 tyrosine kinase (PDB: 3B8Q) domain.



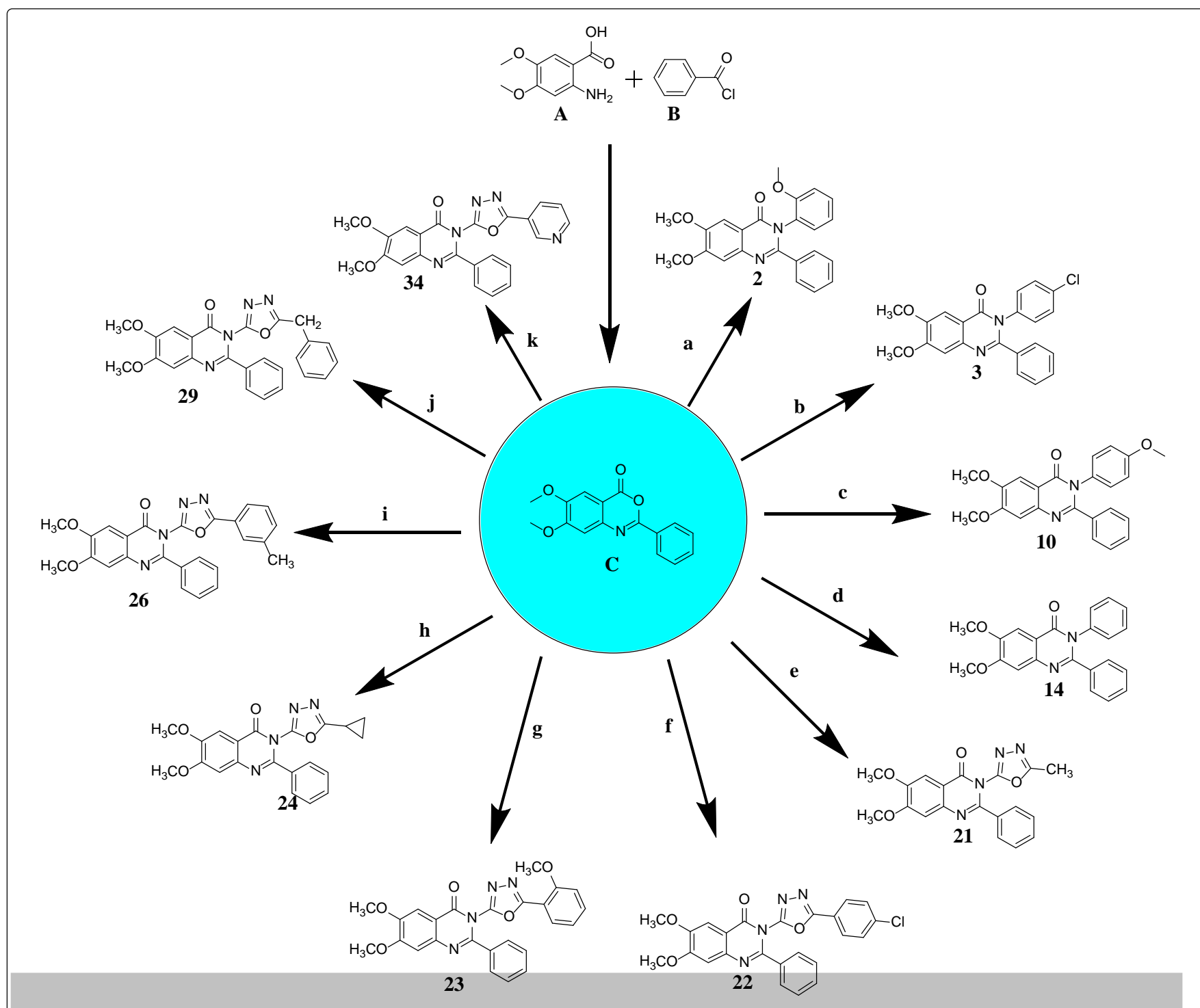


**Fig.10** Binding interaction of Hits with VEGFR-2 tyrosine kinase (PDB: 3B8Q) domain.



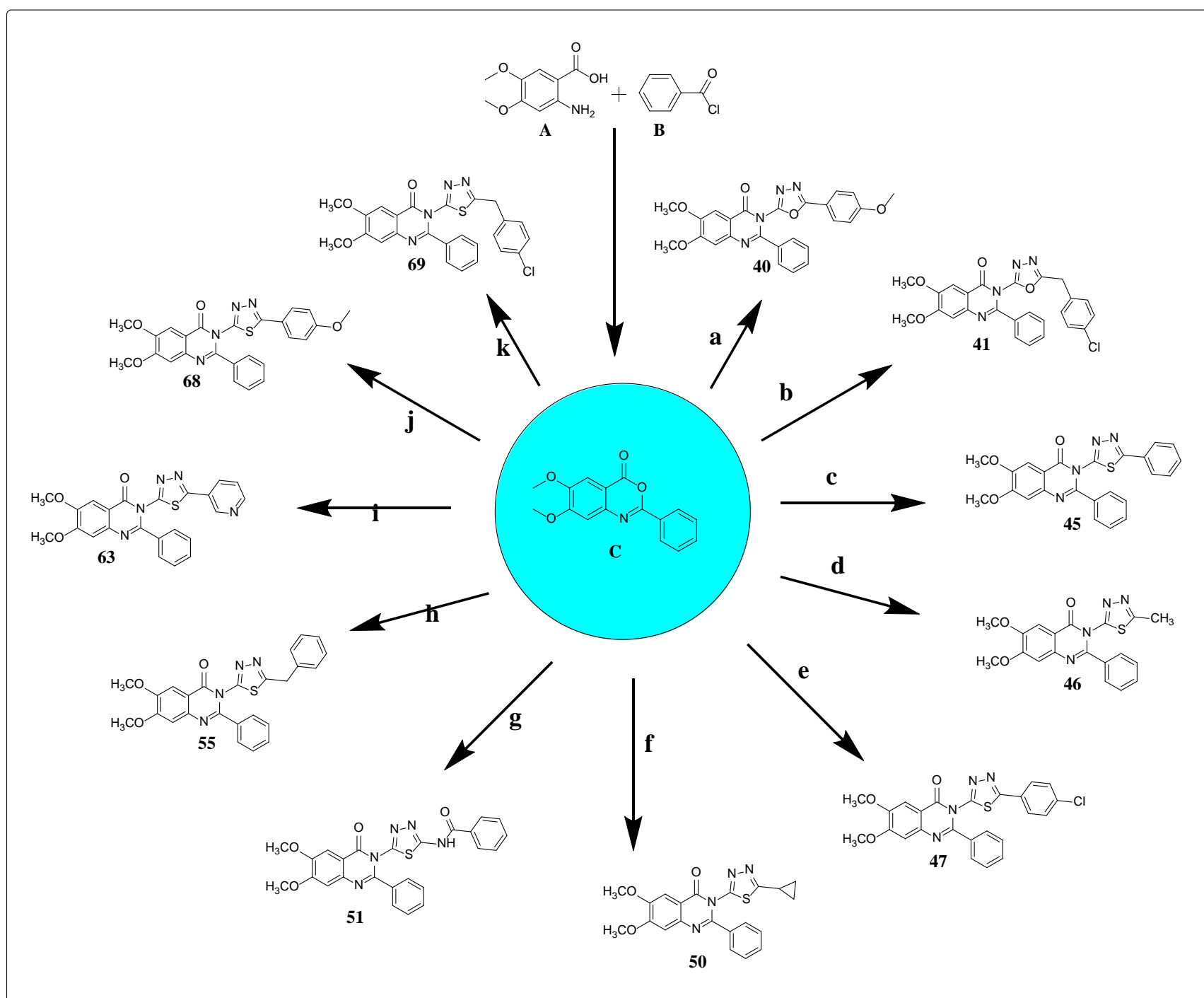


**Fig. 11** Binding interaction of Hits with VEGFR-2 tyrosine kinase (PDB: 3B8Q) domain.



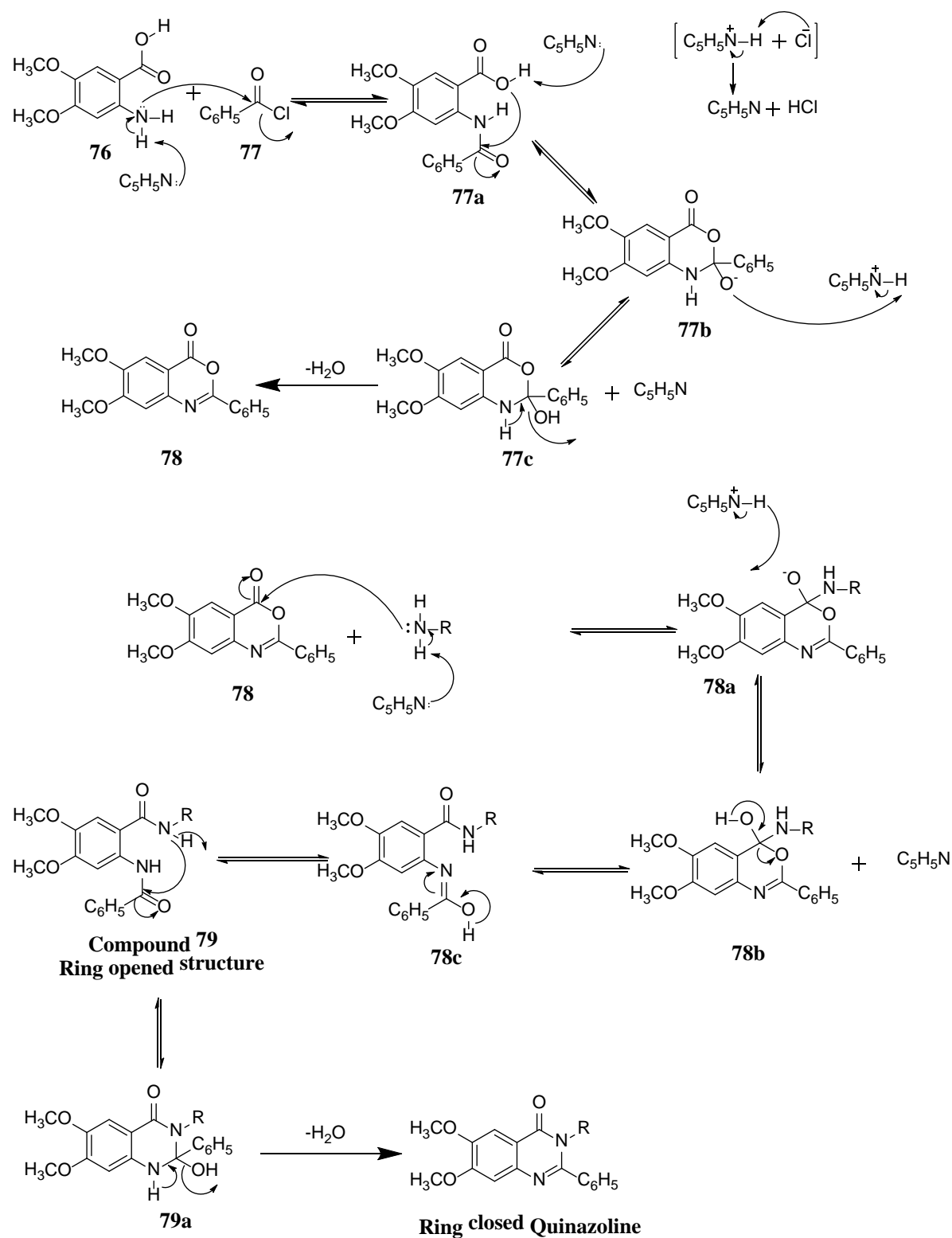
**Scheme 1.** Synthesis of virtually screened compounds

**Reagents:** **a**) 2-methoxyaniline; **b**) 4-chloroaniline; **c**) 4-methoxyaniline; **d**) aniline; **e**) 5-methyl-1,3,4-oxadiazol-2-amine; **f**) 5-(4-chlorophenyl)-1,3,4-oxadiazol-2-amine; **g**) 5-(2-methoxyphenyl)-1,3,4-oxadiazol-2-amine; **h**) 5-cyclopropyl-1,3,4-oxadiazol-2-amine; **i**) 5-m-tolyl-1,3,4-oxadiazol-2-amine; **j**) 5-benzyl-1,3,4-oxadiazol-2-amine; **k**) 5-(pyridin-3-yl)-1,3,4-oxadiazol-2-amine.



**Scheme 2.** Synthesis of virtually screened compounds

**Reagents:** **a**) 5-(4-methoxyphenyl)-1,3,4-oxadiazol-2-amine; **b**) 5-(4-chlorobenzyl)-1,3,4-oxadiazol-2-amine; **c**) 5-phenyl-1,3,4-thiadiazol-2-amine; **d**) 5-methyl-1,3,4-thiadiazol-2-amine; **e**) 5-(4-chlorophenyl)-1,3,4-thiadiazol-2-amine; **f**) 5-cyclopropyl-1,3,4-thiadiazol-2-amine; **g**) N-(5-amino-1,3,4-thiadiazol-2-yl) benzamide; **h**) 5-benzyl-1,3,4-thiadiazol-2-amine; **i**) 5-(pyridin-3-yl)-1,3,4-thiadiazol-2-amine; **j**) 5-(4-methoxyphenyl)-1,3,4-thiadiazol-2-amine; **k**) 5-(4-chlorobenzyl)-1,3,4-thiadiazol-2-amine.



Scheme 3. Reaction mechanism of virtually screened compounds